

DTIC FILE COPY

2

GL-TR-90-0153

AD-A227 423

**Effects of a Descending Lithospheric Slab on Yield
Estimates of Aleutian Nuclear Tests**

**Incorporation of Velocity Gradients in the Synthesis
of Complete Seismograms by the Locked Mode Method**

Vernon F. Cormier

University of Connecticut
Department of Geology and Geophysics
Storrs, Connecticut 06269-2045

August 10, 1990

Scientific Report No. 3

Approved for public release; distribution unlimited

GEOPHYSICS LABORATORY
AIR FORCE SYSTEMS COMMAND
UNITED STATES AIR FORCE
HANSOM AIR FORCE BASE, MASSACHUSETTS 01731-5000

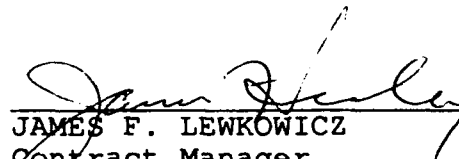
DTIC
ELECTE
OCT 10 1990
S B D
Co

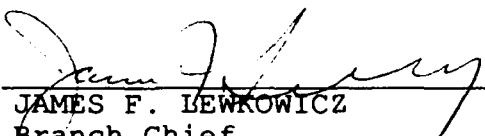
SPONSORED BY
Defense Advanced Research Projects Agency
Nuclear Monitoring Research Office
ARPA ORDER NO 5299

MONITORED BY
Geophysics Laboratory
F19628-88-K-0010

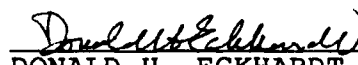
The views and conclusions contained in this document are those of the authors and should not be interpreted as representing the official policies, either expressed or implied, of the Defense Advanced Research Projects Agency or the U.S. Government.

This technical report has been reviewed and is approved for publication.


JAMES F. LEWKOWICZ
Contract Manager
Solid Earth Geophysics Branch
Earth Sciences Division


JAMES F. LEWKOWICZ
Branch Chief
Solid Earth Geophysics Branch
Earth Sciences Division

FOR THE COMMANDER


DONALD H. ECKHARDT, Director
Earth Sciences Division

This report has been reviewed by the ESD Public Affairs Office (PA) and is releasable to the National Technical Information Service (NTIS).

Qualified requestors may obtain additional copies from the Defense Technical Information Center. All others should apply to the National Technical Information Service.

If your address has changed, or if you wish to be removed from the mailing list, or if the addressee is no longer employed by your organization, please notify GL/IMA, Hanscom AFB, MA 01731-5000. This will assist us in maintaining a current mailing list.

Do not return copies of this report unless contractual obligations or notices on a specific document requires that it be returned.

REPORT DOCUMENTATION PAGE

Form Approved
OMB No. 0704-0188

Public reporting burden for this collection of information is estimated to average 1 hour per response, including the time for reviewing instructions, searching existing data sources, gathering and maintaining the data needed, and completing and reviewing the collection of information. Send comments regarding this burden estimate or any other aspect of this collection of information, including suggestions for reducing this burden, to Washington Headquarters Services, Directorate for Information Operations and Reports, 1215 Jefferson Davis Highway, Suite 1204, Arlington, VA 22202-4302, and to the Office of Management and Budget, Paperwork Reduction Project (0704-0188), Washington, DC 20503.

1. AGENCY USE ONLY (Leave blank)		2. REPORT DATE August 10, 1990		3. REPORT TYPE AND DATES COVERED Scientific Report No. 3	
4. TITLE AND SUBTITLE Effects of a Descending Lithospheric Slab on Yield Estimates of Aleutian Nuclear Tests. Incorporation of Velocity Gradients in the Synthesis of Complete Seismograms by the Locked Mode Method.				5. FUNDING NUMBERS PE 61101E PR 8A10 TA DA WU AE Contract F19628-88-K-0010	
6. AUTHOR(S) Vernon F. Cormier					
7. PERFORMING ORGANIZATION NAME(S) AND ADDRESS(ES) University of Connecticut Department of Geology and Geophysics Storrs, CT 06269-2045				8. PERFORMING ORGANIZATION REPORT NUMBER	
9. SPONSORING/MONITORING AGENCY NAME(S) AND ADDRESS(ES) Geophysics Laboratory Hanscom AFB, MA 01731-5000 Contract Manager: James Lewkowicz/LWH				10. SPONSORING/MONITORING AGENCY REPORT NUMBER GL-TR-90-0153	
11. SUPPLEMENTARY NOTES					
12a. DISTRIBUTION/AVAILABILITY STATEMENT Approved for public release; distribution unlimited <i>(Note: See also available for release)</i>				12b. DISTRIBUTION CODE	
13. ABSTRACT (Maximum 200 words) The locked mode method of synthesizing complete regional seismograms (Harvey, 1981) was modified to include the Langer uniform asymptotic approximation to vertical wavefunctions within layers having linear vertical velocity gradients. Good agreement is obtained in gradient models between synthetics computed using the Langer-locked mode method, the colocation method, and the conventional locked mode method in models parameterized by thin homogeneous layers. Errors in calculated displacement introduced by the use of the Langer approximation remain less than several percent for wavelengths $\lambda > 0.2V/VV$. Whenever it is necessary to represent gradients accurately, the Langer-locked mode method is computationally more efficient than the locked mode method using thin homogeneous layers. By reducing the number of parameters needed to describe an Earth model, the Langer-locked mode method will also simplify the inverse problem of determining structure using observed and synthetic regional seismograms. Test calculations of regional seismograms confirm that the Pn and Sn phases are strongly affected by the magnitude of the velocity gradients beneath the Moho, but that Lg is only weakly affected by the details of crustal layering.					
14. SUBJECT TERMS Complete Regional Synthetic Seismograms				15. NUMBER OF PAGES 64	
				16. PRICE CODE	
17. SECURITY CLASSIFICATION OF REPORT UNCLASSIFIED	18. SECURITY CLASSIFICATION OF THIS PAGE UNCLASSIFIED	19. SECURITY CLASSIFICATION OF ABSTRACT UNCLASSIFIED	20. LIMITATION OF ABSTRACT SAR		

TABLE OF CONTENTS

I. <i>Technical Summary</i>	
II. <i>Incorporation of Velocity Gradients in the Synthesis of Complete Seismograms by the Locked Mode Method</i>	
1. <i>Abstract</i>	Page 1
2. <i>Introduction</i>	Page 2
3. <i>Review of the Locked Mode Method</i>	Page 4
4. <i>The Accuracy of the Langer Approximation</i>	Page 7
5. <i>Intrinsic Attenuation</i>	Page 9
6. <i>Effects of Gradients in Realistic Models</i>	Page 13
7. <i>Conclusions</i>	Page 14
8. <i>Acknowledgements</i>	Page 16
9. <i>References</i>	Page 17
III. <i>Appendix I - The Langer Approximation</i>	Page 21
1. <i>Vertical Slownesses</i>	Page 23
2. <i>Branch Cuts and Complex P</i>	Page 24
3. <i>Fundamental Matrices</i>	Page 25
4. <i>P-SV</i>	Page 25
5. <i>Fundamental Matrix for SH Propagation</i>	Page 26
6. <i>Model Parameterization</i>	Page 26
IV. <i>Appendix II - Mode Amplitude and Eigenfunctions</i>	Page 28
1. <i>Rayleigh Modes</i>	Page 28
2. <i>The Y Matrix</i>	Page 28
3. <i>Layer Reduction</i>	Page 32
4. <i>Eigenfunctions</i>	Page 32
5. <i>Love Modes</i>	Page 34
6. <i>Eigenfunctions</i>	Page 35
V. <i>Figures (1-10)</i>	Page 36



iii

Accession For	
NTIS GRA&I	<input checked="" type="checkbox"/>
DTIC TAB	<input type="checkbox"/>
Unannounced	<input type="checkbox"/>
Justification	
By _____	
Distribution/	
Availability Codes	
Dist	Avail and/or Special
A-1	

TECHNICAL SUMMARY

The objective of this project is to determine the yield bias of underground nuclear tests induced by the presence of a high velocity descending slab beneath the test site. Specifically, the effect of the Aleutian slab is being investigated on the US underground tests Longshot, Milrow, and Cannikan. P wave seismograms will be synthesized using dynamic ray tracing and superposition of Gaussian beams in three-dimensional models of the Aleutian slab determined from P travel time delays. Focusing and defocusing and multipathing at teleseismic distances will be evaluated by comparison of observed with synthetic seismograms of the Aleutian tests.

Data collection for of Amchitka P waveforms and amplitudes was initiated. A no cost extension of this project was requested and granted by AFGL to allow for collection of the necessary data to complete the project. Pending completion of the data collection, work was begun on a project to compute complete regional seismograms in crustal and upper mantle models having gradients in layers. This project will be included in a new proposal and directly contributes to the AFGL treaty verification program, with its current emphasis on CTBT monitoring at local and regional distances.

In collaboration with Danny Harvey, the locked mode method of synthesizing complete regional seismograms (Harvey, 1981) was modified to include the Langer uniform asymptotic approximation to vertical wavefunctions within layers having linear vertical velocity gradients. Good agreement is obtained in gradient models between synthetics computed using the Langer-locked mode method, the colocation method, and the conventional locked mode method in models parameterized by thin homogeneous layers. Errors in calculated displacement introduced by the use of the Langer approximation remain less than several percent for wavelengths $\lambda \leq 0.2V/\nabla V$. Whenever it is necessary to represent gradients accurately, the Langer-locked mode method is computationally more efficient than the locked mode method using thin homogeneous layers. By reducing the number of parameters needed to describe an Earth model, the Langer-locked mode method will also simplify the inverse problem of determining structure using observed and synthetic regional seismograms. Test calculations of regional seismograms confirm that the Pn and Sn phases are strongly affected by the magnitude of the velocity gradients beneath the Moho, but that Lg is only weakly affected by the details of crustal layering.

INCORPORATION OF VELOCITY GRADIENTS IN THE
SYNTHESIS OF COMPLETE SEISMOGRAMS BY THE LOCKED MODE METHOD

V.F. Cormier¹ and D. Harvey²

¹ Department of Geology and Geophysics

University of Connecticut, Box U-45

Storrs, CT 06269-2045

²CIRES

University of Colorado

Boulder, CO 80309

ABSTRACT

Any realistic crustal and upper mantle model possesses layers with vertical gradients. Elastic moduli and density in each layer are affected by pressure, temperature, pore fluids, and crack density. All of these quantities change continuously with depth, many having a well known functional dependence on depth. Virtually all of the regional phases can be strongly affected by velocity gradients. The best known effects of velocity gradients are on the Pn and Sn , in which small changes in the velocity gradient beneath the Moho can make large changes in the decay of Pn and Sn with distance. Methods of synthesizing complete regional seismograms often inadvertently ignore the effect of crustal gradients by parameterizing the Earth model with planar homogeneous layers. To remedy this problem we have modified the locked mode method of synthesizing complete regional seismograms to include the Langer uniform asymptotic approximation to vertical wavefunctions within

layers having linear vertical velocity gradients. Good agreement is obtained in gradient models between synthetics computed using the Langer-locked mode method, the colocation method, and the conventional locked mode method in models parameterized by thin homogeneous layers. Errors in calculated displacement introduced by the use of the Langer approximation remain less than several percent for wavelengths $\lambda \leq 0.2V/\nabla V$. Whenever it is necessary to represent gradients accurately, the Langer-locked mode method is computationally more efficient than the locked mode method using thin homogeneous layers. By reducing the number of parameters needed to describe an Earth model, the Langer-locked mode method will also simplify the inverse problem of determining structure using observed and synthetic regional seismograms. Test calculations of regional seismograms confirm that the Pn and Sn phases are strongly affected by the magnitude of the velocity gradients in beneath the Moho, but that Lg is only weakly affected by the details of crustal layering.

INTRODUCTION

Complete seismograms at local and regional distances are now routinely computed in plane layered models for a variety of source receiver geometries, source depths, and source types by integrating or summing over wavenumbers (Bouchon and Aki, 1977; Kind 1978; Wang and Hermann, 1980) or summing locked or leaky modes (Harvey, 1981; Kerry, 1981; Haddon, 1986; Nolet et al., 1989). The computational expense of these calculations remains relatively cheap as long as the crust and upper mantle model can be described by a small number of planar, homogeneous layers.

Seismograms synthesized in models composed of small number of plane homogeneous layers

ignore the continuous depth dependence of elastic moduli. Usually seismograms are synthesized in simple models composed of a two or three homogeneous layers of crust overlaying a homogeneous lid, low velocity zone, and upper mantle beneath the lid. Since Earth curvature is ignored in these calculations, the model is effectively one in which each layer has a small negative gradient with depth.

The simplest generalization of a homogeneously layered model is to allow for the effect of velocity gradients. Any realistic crustal and upper mantle model possesses layers with vertical gradients. Elastic moduli and density in each layer are affected by pressure, temperature, pore fluids, crack density and aspect ratio. All of these quantities change continuously with depth, many having a well known functional dependence on depth.

Virtually all of the regional phases can be strongly affected by velocity gradients. One example is dispersion of the fundamental mode Rayleigh wave, or R_g phase at local and regional distances. Crustal models having a homogeneous layer at the surface produce an unrealistically impulsive, undispersed R_g arrival. To match observed data, the fundamental mode arrival must be artificially removed or attenuated. Perhaps the best known effects of gradients on regional phases are those on the P_n and S_n phases. In a plane layered model, the P_n and S_n phases are classical head waves traveling just beneath the Moho. Hill (1971) and Červený and Ravindra (1971) have shown how gradients transform classical headwaves into interference headwaves or "whispering gallery waves" (e.g., Cormier and Richards, 1976; Menke and Richards, 1980). The distance decay of both classical and interference headwaves is frequency dependent.

In this paper, we describe the results of incorporating velocity gradients in crustal and upper

mantle models using the locked mode method. Gradients are introduced into the computations by allowing each layer to be vertically inhomogeneous and applying the Langer approximation (Appendix I) to calculate an asymptotic approximation in frequency to the vertical wavefunctions in each inhomogeneous layer.

A brief review of the locked mode method is first given. Mathematical details of the Langer approximation and its incorporation in the locked mode method are described in Appendices I and II. The remainder of the paper describes the results of tests conducted to determine the accuracy of the Langer approximation and how it breaks down as the gradient in the layer increases. A discussion and example show how depth and frequency dependent attenuation can be included in the Langer-locked mode method. The paper concludes with discussion of synthetic seismographs showing how gradients near the free surface and Moho can radically affect the propagation of some of the principal regional phases.

Review of the Locked Mode Method

Following Harvey (1981; 1985), the complex displacement spectra are evaluated from

$$R u(\omega, x_r, \theta_r, z_r) = -R_\alpha I - R_\beta I - i \sum_n \sum_m R \Lambda(n, \omega) R \Sigma^T(n, \omega, m) R E(n, \omega, z_s) R \hat{\psi}(n, \omega, m, x_r, \theta_r, z_r) \quad (1)$$

$$L u(\omega, x_r, \theta_r, z_r) = -L_\rho I - i \sum_n \sum_m L \Lambda(n, \omega) L \Sigma^T(n, \omega, m) L E(n, \omega, z_s) L \hat{\psi}(n, \omega, m, x_r, \theta_r, z_r)$$

where the subscripts R and L denote Rayleigh and Love modes respectively.

${}_R\Lambda$ and ${}_L\Lambda$ area scalar amplitude factors defined by

$${}_R\Lambda(n, \omega) = -\frac{{}_RkY_{23}(0)}{\partial Y_{12}(0)/\partial k} \quad (2)$$

$${}_L\Lambda(n, \omega) = -\frac{{}_LkD_2(0)}{\partial D_1(0)/\partial k}$$

${}_R\Sigma^T$ and ${}_L\Sigma^T$ are row vectors defined from the source jump vectors. ${}_R\hat{\psi}$ and ${}_L\hat{\psi}$ are defined from products of eigenfunctions for displacement $({}_RE_1, {}_RE_2)$ and ${}_LE)_1$ and vector cylindrical harmonics $\hat{P}, \hat{B}, \hat{C}$:

$${}_R\hat{\psi}(n, \omega, m, x_r, \theta_r, z_r) = {}_RE_1(n, \omega, z_r)\hat{P}(n, \omega, m, x_r, \theta_r) + {}_RE_2(n, \omega, z_r)\hat{B}(n, \omega, m, x_r, \theta_r) \quad (3)$$

$${}_L\hat{\psi}(n, \omega, m, x_r, \theta_r, z_r) = {}_LE_1(n, \omega, z_r)\hat{C}(n, \omega, m, x_r, \theta_r)$$

${}_R{}_aI$ and ${}_L{}_sI$ are branch cut integrals, which account for energy that cannot be represented by normal modes, and are associated with near vertically propagating P and S waves that leak into the halfspace. The locked mode method does not evaluate the branch cut integrals. It chooses the halfspace to be sufficiently deep and fast such that all of the energy important to a particular time window at a particular distance can be accurately represented by the locked mode summation alone.

Seismograms are synthesized by evaluating the complex spectra at discrete frequencies and inverting to the time domain by fast Fourier transform. A small complex frequency can be added to attenuate all arrivals that arrive outside of the finite time window given by the folding frequency

of the discrete Fourier transform (Rosenbaum, 1974; Müller and Schott, 1981). Harvey (1981, 1985) gives detailed derivations of the locked mode method and describes its implementation in media described by homogeneous layers. The principal modifications of the method for use with the Langer approximation are concerned with the calculation of the eigenfunction vector E and the scalar amplitude factors $R\Lambda$ and $L\Lambda$. The partial derivatives with respect to k appearing in the amplitude factors are calculated by difference derivatives. Appendices I and II describe the calculation with the Langer approximation of the Y matrix elements and the vectors D and E .

The Langer approximation can also be implemented in methods of synthesizing complete seismograms that numerically integrate over horizontal wavenumber and slowness (Cormier, 1980). The primary advantage of the locked mode method is that most of the computational effort involved in the calculation of the amplitude factors and eigenfunctions can be catalogued for use with different source-receiver geometries and different moment tensor representations of point sources. Although response functions can be similarly catalogued in approaches that integrate or sum over wavenumber or slowness, this is rarely done in practice. A secondary advantage of the locked mode method is that a large body of literature exists in modal notation on inversion for structure and source parameters. The analysis of problems using normal modes of the whole Earth at low frequency and long range can usually be directly adapted to higher frequency and shorter range using locked modes (e.g., Gombert and Masters, 1988).

The Accuracy of the Langer Approximation

The Langer approximation assumes decoupling between P and S waves and up- and down-going waves in each gradient layer, and the criteria for its accuracy are thus similar to those used in ray-asymptotic solutions to the elastodynamic equation of motion in inhomogeneous media (Richards, 1976). Qualitatively, the Langer approximation is known to become less accurate as non-dimensional ratios $\lambda/(v/\nabla v)$ increase, where v is a P or S velocity or density (Richards, 1976; Chapman, 1974). Another way in which this is commonly phrased is that the wavelength must be much smaller than the scalelength of the medium, l , where l is the maximum of $(\alpha/\nabla\alpha, \beta/\nabla\beta, \rho/\nabla\rho)$ (Beydoun and Ben-Menahem, 1985). A goal in this study was to quantify the breakdown in the Langer approximation as the scalelength of gradient layers decrease, determining exactly how large the ratio λ/l can be before errors in calculated displacement exceed some specified bound.

The first step in such a study is to choose accurate reference synthetic seismograms in models having strong gradients. Spudich and Ascher (1983) published synthetic seismograms calculated by the numerical collocation method for a simple model consisting of a gradient over half space. The gradient layer in this model was parameterized by a sequence of 40 thin layers (Figure 1), the width of each thin layer approximately equal to one-tenth the wavelength of shear waves at 1 Hz. Excellent agreement was found between the locked mode synthetics and the collocation synthetics. This result confirmed that locked mode synthetics computed in models in which gradient layers are represented by thin layers can be used as accurate reference synthetics to test the Langer approximation.

To test the accuracy of the Langer approximation, seismograms were synthesized using the

locked mode method using the Langer approximation in a series of models with increasing gradients in P and S velocity and density in a layer over a halfspace (Figure 2). Figure 3 compares the dispersion curves of the locked Love and Rayleigh modes calculated with Langer approximation in a thick continuous gradient layer with those calculated by parameterizing the gradient layer with thin homogeneous layers. Even for the most severe of the gradients shown in Figure 2, the dispersion curves calculated using the Langer approximation remain quite accurate throughout nearly the entire range of phase velocity and frequency. The primary region of error occurs for the low frequencies of the fundamental mode. This is not unexpected since most of the energy of the fundamental mode in this frequency band is confined to the strong gradient layer near the surface. As expected, the errors in the dispersion curves calculated by the Langer approximation are largest at low frequency, where the wavelength approaches the scale length of the gradient layer.

Figure 4 compares reference synthetics and Langer approximated synthetics for the sequence of gradient models shown in Figure 2. Although the kinematic errors in the mode dispersion calculations are small throughout most of the frequency band, the dynamic errors in mode amplitudes are sufficient to produce poor matches in the group velocity band corresponding to the fundamental mode and the first few higher modes. These effects can be seen in Figure 4, in which the early portion of the seismograms computed by the two methods are more closely in phase but become progressively out of phase in the time window corresponding to the arrival of the fundamental mode and first few higher modes. The agreement between the two methods is much better for the transverse component than the radial or vertical components of motion.

The match between reference and Langer approximated synthetics becomes nearly perfect for

weakest surface gradients (model 3 in Figure 2). The seismograms computed by the two methods overlay one another to within the thickness of plotted lines. The difference seismograms in Figure 5 are largest near the peak oscillations where small differences in arrival time of pulses having high slopes produce large differences. Since the dominant frequency the synthetic seismograms is about 0.5 Hz., one can conclude that errors in the use of the Langer approximation become less than several percent when the ratio λ/l is less than or equal to 0.2. If one were not interested in the accuracy of the fundamental mode at frequencies less than 1 Hz, the Langer approximation could synthesize the higher modes in this example with high accuracy across the entire frequency band. The fundamental mode could be synthesized with high accuracy at frequencies greater than 1 Hz.

Intrinsic Attenuation

To be practically useful, any method of synthesizing complete seismograms at local and regional distances must be capable of including intrinsic attenuation. The incorporation of the attenuation in the Langer approximation simply consists of the analytic continuation of all formulae to complex velocities (Cormier and Richards, 1976, 1989). Care must be exercised in the definition of branch cuts of square roots and fractional powers appearing in both the analytic expressions and function subroutines used in evaluating the Langer approximation (see Appendix I), but this is not an insurmountable problem. The Langer subroutine modified for use with locked mode calculations has been tested in problems involving integration in the complex ray parameter plane combined with complex, frequency dependent velocity. It returns generalized vertical wavefunctions and slownesses that are continuous in the complex ray parameter plane except for poles and branch

cuts, which emanate from complex ray parameters corresponding to grazing incidence on boundaries in an anelastic model. Test calculations have demonstrated that the position of these singularities do not impede a successful search for the complex zeros of the dispersion functions of locked modes in an anelastic model.

An absorption band model of attenuation is assumed (e.g., Lundquist and Cormier, 1980). At any radian frequency ω in this model, the complex velocity is given by

$$\beta(\omega) = \beta_r \sqrt{\frac{1 + 2/\pi Q_\beta^{-1} A_\omega}{1 + 2/\pi Q_\beta^{-1} A_r}} \quad (4)$$

where

$$A_\omega = \ln \left(\frac{i\omega + \omega_1}{i\omega + \omega_2} \right) \quad (5)$$

$$A_r = \ln \left(\frac{i\omega_r + \omega_1}{i\omega_r + \omega_2} \right)$$

β_r is the real velocity at a reference frequency ω_r . Complex P velocity α is calculated by the same formula, with an option to constrain attenuation to be pure shear or to specify a different peak attenuation parameter Q_α^{-1} for P waves. Ideally the reference frequency ω_r should be chosen to be in the middle of the frequency band of the seismic data used in determining a trial model for a given region. Complex velocities are calculated at each layer boundary by equation 5 above and linear gradients of complex velocity are assumed in each layer. The delay time function τ needed by the Langer approximation is calculated as described in Appendix II, but it now must be recalculated at each frequency. It is possible to specify different peak Q_β values as well as

different upper and lower limits, ω_1 and ω_2 , of the relaxation band at the top and bottom of each inhomogeneous layer.

A test anelastic model is shown in Figure 6. The attenuation model is an absorption band model in pure shear attenuation having gradients in peak attenuation Q_β^{-1} , and low and high frequency corners, ω_1, ω_2 , of the relaxation band. A minimum value of $Q_\beta = 20$ is assumed at the surface. The velocities and Q values are similar to values measured from regional seismograms in New England (Kafka and Reiter, 1987). Locked mode seismograms were synthesized in these model using two different approaches. In the first approach, only the real part of the complex velocities was used in calculation of mode amplitudes and eigenfunctions, a complex phase velocity was substituted in the cylindrical harmonics describing the horizontal propagation of each mode. This complex phase velocity is taken from the complex pole k estimated by first order perturbation theory. This is the standard approach for handling attenuation in surface wave and locked mode calculations (Harvey, 1985; Panza and Sudhadolc, 1987), and is assumed to be accurate if the Q factor is sufficiently high. Day et al. (1989) have shown this approach to be inaccurate for some regional seismic phases even at Q values on the order of several hundred. For this reason, seismograms were also synthesized by an exact approach, in which a search was made for the complex roots of the dispersion function and all formulae, including amplitude factors and eigenfunctions, were evaluated at these complex roots. The complex pole searching algorithm was based on one suggested by Schwab and Knopoff (1971), with modifications near osculating points of the dispersion curves. Near these points, the complex roots are found by the same algorithm for a series of increasing Q^{-1} values, approaching the true Q^{-1} model. Checks are made for duplication or omission of poles at the end of this procedure for

each frequency.

Figure 7 compares the results of these two methods for incorporating attenuation of the fundamental mode Rayleigh wave. The seismograms computed by the different methods nearly overlay one another at all distances. The exact method reduces some high frequency numerical noise, which is barely visible at the scale of Figure 7. The differences in the complex phase velocities computed by the two methods are on the order of 0.001 km/sec in the real part of the complex phase velocity and vary from 1×10^{-10} to 1×10^{-4} km/sec in the complex part of phase velocity as frequency increases up to 2 Hz. The differences between the depth behavior of the real part of the complex eigenfunctions are insignificant between the two methods. From these results it can be concluded that the perturbation approach to attenuation remains very accurate in the synthesis of the fundamental mode for Q values as low as 20. For the synthesis of higher modes, particularly those contributing to refracted P and S and interference head waves, more detailed tests have shown that the perturbation approach introduces significant error as Q values decrease below several 100.

It is reasonable to assume that gradients in the real part of elastic moduli are also associated with gradients in the imaginary part of elastic moduli. We have demonstrated in this section that the Langer approximation can be applied to locked mode calculations in models having gradients in complex elastic moduli. Often a very low Q layer is required in a surface layer in order to produce realistic simulations of seismograms observed at local and regional distances (e.g., Panza and Sudhacolc, 1987). If the apparent attenuation of such a layer is truly due to viscoelasticity, its effects can be accurately calculated by complex locked modes. It is worth noting, however, that such apparent low Q 's are likely due to a combination of scattering by topography of layer

boundaries and volumetric heterogeneities and frictional sliding of grains and open cracks. Neither of these effects can be simulated by a combination of vertically varying layers and linear viscoelastic relaxations.

Effects of Gradients in Realistic Models

To test the effects of crustal and upper mantle gradients on regional seismic phases, locked mode synthetics were computed in two simple models MH and MG (Figure 8). Model MH consists of a two-layered crust overlaying a homogeneous mantle. MH has also been used for testing and benchmark timing of many different techniques of computing complete seismograms at regional distances (Richards and Mithal, personal communications). Model MG consists of a single crustal layer having a positive gradient with depth, overlaying a mantle having a positive gradient with depth. The mantle gradient is consistent with the increase in seismic velocities typical of reference earth models between the Moho and 400 km depth. The depth averaged crustal velocities of MH and MG are identical. Both models have an attenuation structure, with Q 's in a high enough range that simple perturbation theory can be accurately used to calculate the effects of attenuation in the locked mode method. Seismograms were synthesized in a frequency band up to 2 Hz. for the source and receiver geometries used by W-Y. Kim (1987), who synthesized seismograms in model MH using wavenumber integration.

The synthetic seismograms for the first 10 Rayleigh modes (Figure 9) are very similar for both model MH and MG. The group velocity window of the energy centroid corresponds to that expected for the L_g phase. The strong similarity of the synthetic seismograms suggests that L_g is not very

sensitive to the details of the crustal model, its coda primarily being controlled by the total thickness of the crust and its average shear velocity. It is probably possible to simulate realistic Lg phases using a very few number of crustal layers. Introduction of crustal layers in a modeling experiment may not be necessary unless there is compelling evidence for crustal discontinuities observed in the earlier time window in the form of refracted body waves and interference head waves.

In a comparison of complete seismograms (Figure 10), the seismograms are very similar at closer ranges but at 300 km some differences begin to be notable. Pn and Sn are very weak in the MH simulation, but are very strong in the MG synthetic. Pn, Sn, and crustal reverberations converted to Pn and Sn are so strong in the MG synthetic that they dominate Lg in amplitude, and the seismogram seems to be a series of spikes when the display is scaled on the peak amplitude. The comparison confirms what is known about Pn and Sn as interference head waves in models having positive gradients below the Moho. A positive gradient acts to enhance the amplitude of the interference head wave far above what would be predicted for a classical head wave in a homogeneous layer (Hill, 1971; Cerveny and Ravindra, 1971; Menke and Richards, 1980).

CONCLUSIONS

In this paper, we have demonstrated that even small gradients of $\nabla V = 0.03 \text{ sec.}^{-1}$ can substantially affect the distance decay of interference head waves such as Pn and Sn. Lg, on the other hand, is only very weakly sensitive to details of crustal layering or gradients. The peak amplitude and coda length of Lg primarily depends on total crustal thickness and average shear velocity of the crust.

In either a locked mode or wavenumber integration approach to synthesizing complete seismo-

grams, the Langer approximation can accurately approximate vertical wavefunctions in inhomogeneous layers having a single ray turning point for wavelengths that are small with respect to the scale length of the layer. This result can be quantified by stating that errors in the amplitude and phase of synthetic seismograms are less than several per cent for wavelengths $\lambda \leq 0.2V/\nabla V$, where V is a velocity or density function. At 5 Hz. this inequality is satisfied by gradients beneath the Moho as high as 0.8 sec.^{-1} .

Propagation of the wavefield using the Langer approximation in a vertically inhomogeneous layer will often represent a computational savings over propagation through the gradient layer parameterized by a sequence of thin layers. An example of a gradient layer parameterized by 40 thin homogeneous layers executed about a factor of two slower in both the pole searching and eigenfunction evaluation compared to the same calculations using the Langer approximation in the gradient layer parameterized by analytic velocity functions. A calculation in a thick homogeneous layer, however, would still always be more efficient than a calculation using the Langer approximation in an inhomogeneous layer of the same thickness. A model parameterization that may be the best compromise between computational efficiency and realism in the behavior of regional phases would be one having a crust composed of homogeneous layers overlaying a mantle composed of gradient layers. Seismograms synthesized in such a model could accurately predict the Lg phase as well as the Pn and Sn phases. (This study did not investigate the importance of crustal gradients for the Pg phase.)

The Langer locked mode approach to synthesizing complete seismograms may also offer some advantages in waveform inversion for earth structure. By reducing the number of parameters needed

to describe a model, the inverse problem for structure would be simplified and fewer experiments would be needed to determine the maximum number of resolvable layers. A layer need only be introduced whenever the data firmly suggest the existence of first order discontinuities.

ACKNOWLEDGEMENTS

During the course of this reaseach, we appreciated and benefited from suggestions and comments by Charles Archambeau and Paul Richards. This research was supported by the Advanced Research Projects Agency of the Department of Defense, monitored by the Geophysics Laboratory under contract F19628-88-K-0010.

REFERENCES

- Abo-Zena, A., Dispersion function computations for unlimited frequency values, *Geophys. J. R. Astron. Soc.*, 58, 91-105, 1979.
- Aki, K., and P.G. Richards, *Quantitative Seismology: Theory and Methods*, W.A. Freeman and Co., San Francisco, 1980.
- Beydoun, W.B., and A. Ben-Menahem, Range of validity of seismic ray and beam methods in general inhomogeneous media, I and II, *Geophys. J. R. Astron. Soc.*, 82, 207-262, 1985.
- Bouchon, M., and K. Aki, Discrete wave number representation of seismic source wave fields, *Bull. Seism. Soc. Am.*, 67, 259-277, 1977.
- Červený, V., and J. Jansky, Ray amplitudes of seismic body waves in inhomogeneous, radially symmetric media, *Stud. Geophys. Geod.*, 27, 9-18, 1983.
- Červený, V., and R. Ravindra, *Theory of Seismic Headwaves*, University of Toronto Press, 1971.
- Chapman, C.H., The turning point of elastodynamic waves, *Geophys. J. R. Astron. Soc.*, 39, 613-622, 1974.
- Cormier, V.F., and P.G. Richards, Comments on "The Damping of Core Waves" by Anthony Qamar and Alfredo Eisenberg, *J. Geophys. Res.*, 81, 3066-3068, 1976.
- Cormier, V.F., Full wave theory applied to a discontinuous velocity increase: the inner core boundary, Ph.D. Thesis, Columbia University, 1976.
- Cormier, V.F., Ph.D. Thesis, Columbia University, 1976.
- Cormier, V.F., The synthesis of complete seismograms in an Earth model specified by radially inhomogeneous layers, *Bull. Seismol. Soc. Am.*, 70, 691-716, 1980.

- Cormier, V.F., and P.G. Richards, Full wave theory applied to a discontinuous velocity increase: the inner core boundary, *J. Geophys.*, **43**, 3-31, 1977.
- Cormier, V.F., and P.G. Richards, Spectral synthesis of body waves in earth models specified by vertically varying layers, In: *Seismological Algorithms*, D. Doornbos (ed.), Academic Press, 1989.
- Day, S.M., K.L. McLaughlin, B. Shkoller, and J.L. Stevens, Potential errors in locked mode synthetics for anelastic earth models, *Geophys. Res. Lett.*, **16**, 203-206, 1989.
- Doornbos, D.J., The effect of a second order velocity discontinuity on elastic waves near their turning point, *Geophys. J. R. Astron. Soc.*, **64**, 499-511, 1981.
- Gomberg, J.S., and T.G. Masters, Waveform modelling using locked-mode synthetic and differential seismograms, *Geophys. J.*, **94**, 193-218, 1988.
- Haddon, R.A.W., Exact evaluation of the response of a layered elastic medium to an explosive point source using leaking modes, *Bull. Seism. Soc. Am.*, **76**, 1755-1775, 1986.
- Harvey, D., Seismogram synthesis using normal mode superposition: the locked mode approximation, *Geophys. J. R. Astr. Soc.*, **66**, 37-61, 1981.
- Harvey, D., A spectral method for computing synthetic seismograms, Ph.D. Thesis, University of Colorado, 1985.
- Hill, D.P., Velocity gradients and anelasticity, *J. Geophys. Res.*, **76**, 3309-3325, 1971.
- Kafka, A., and E.C. Reiter, Dispersion of Rg waves in southeastern Maine: evidence for lateral anisotropy in the shallow crust, *Bull. Seism. Soc. Am.*, **77**, 925-941, 1987.
- Kerry, N., Synthesis of seismic surface waves, *Geophys. R. Astron. Soc.*, **64**, 425-446, 1981.
- Kim, W.-Y., Modelling short-period crustal phases at regional distances for seismic source-parameter

- inversion, *Phys. Earth Planet. Int.*, **47**, 159-178, 1987.
- Kind, R., The reflectivity method for a buried source, *J. Geophys. Res.*, **44**, 603-612, 1978.
- Langer, R.E., On the asymptotic solutions of differential equations, with an application to the Bessel functions of large complex order, *Trans. Am. Math. Soc.*, **34**, 447-480, 1932.
- Langer, R.E., The asymptotic solutions of ordinary linear differential equations of the second order, with special reference to a turning point, *Trans. Am. Math. Soc.*, **67**, 461-490, 1949.
- Lundquist, G.M., and V.F. Cormier, Constraints on the absorption band model of Q, *J. Geophys. Res.*, **85**, 5244-5256, 1980.
- Menke, W.H., and P.G. Richards, Crust-mantle whispering gallery phases: a deterministic model of *P_n* wave propagation, *J. Geophys. Res.*, **85**, 5416-5422, 1980.
- Müller, G., Approximate treatment of elastic body waves in media with spherical symmetry, *Geophys. J. R. Astron. Soc.*, **23**, 435-449, 1971.
- Müller, G., and W. Schott, Some recent extensions of the reflectivity method, In: *Identification of Seismic Sources - Earthquake or Underground Explosion*, pp. 347-372, Nato Advanced Study Institutes Series, Reidel Publishing Co., 1981.
- Nolet, G., R. Sleeman, V. Nijhof, and B.L.N. Kennett, Synthetic reflection seismograms in three dimensions by a locked-mode approximation, *Geophysics*, **54**, 350-358, 1989.
- Panza, G.F., and P. Sudhadolc, Complete strong ground motion synthetics, In: *Strong Ground Motion Synthetics*, B. Bolt (ed.), pp. 153-204, Academic Press, 1987.
- Richards, P.G., Weakly coupled potentials for high frequency elastic waves in continuously stratified media, *Bull. Seism. Soc. Am.*, **64**, 1575-1588, 1974.

- Richards, P.G., On the adequacy of plane wave reflection/transmission coefficients in the analysis of seismic body waves, *Bull. Seismol. Soc. Am.*, 66, 701-717, 1976.
- Rosenbaum, J.H., Synthetic microseisms; logging in porous formations, *Geophysics*, 39, 14-32, 1974.
- Schwab, F., and L. Knopoff, Surface waves in multilayered anelastic media, *Bull. Seism. Soc. Am.*, 61, 893-912, 1971.
- Spudich, P., and U. Ascher, Calculation of complete theoretical seismograms in vertically varying media using collocation methods, *Geophys. J. R. Astron. Soc.*, 75, 101-124, 1983.
- Wang, C.Y., and R.B. Hermann, A numerical study of P-, SV-, and SH-wave generation in a plane layered medium, *Bull. Seism. Soc. Am.*, 70, 1015-1036, 1980.
- Woodhouse, J.H., Asymptotic results for elastodynamic propagator matrices in plane stratified and spherically stratified Earth models, *Geophys. J. R. Astron. Soc.*, 54, 263-291, 1978.

APPENDIX I – THE LANGER APPROXIMATION

Vertical Wavefunctions

The notation for the Langer approximation (Langer, 1932; 1949) differs among different authors who have applied it to seismic wave propagation. (Richards, 1976; Woodhouse, 1978; Chapman, 1974; Doornbos, 1981), involving either Hankel functions of order 1/3 or Airy functions of different types or arguments to give exponentially decaying and growing type solutions below a turning point. The notation adopted here is basically that given in Aki and Richards (1980).

The Langer approximation is a uniformly asymptotic approximation to the vertically separated part of the solution to the elastodynamic wave equation in a region in which elastic moduli and density vary continuously with depth. The zeroth order term in frequency in the asymptotic solution is given as

$$\begin{aligned}
 \pi^{(1)}(r) &= \sqrt{2\pi} e^{-\frac{i\pi}{3}} \left(\frac{\zeta_\alpha^{1/4}}{\lambda_\alpha^{1/2}} \right) \text{Ai}(-e^{\frac{2i\pi}{3}} \zeta_\alpha) \\
 \pi^{(2)}(r) &= \sqrt{2\pi} e^{\frac{i\pi}{3}} \left(\frac{\zeta_\alpha^{1/4}}{\lambda_\alpha^{1/2}} \right) \text{Ai}(-e^{-\frac{2i\pi}{3}} \zeta_\alpha) \\
 \pi^{(3)}(r) &= \sqrt{2\pi} \left(\frac{\zeta_\alpha^{1/4}}{\lambda_\alpha^{1/2}} \right) \text{Ai}(-\zeta_\alpha) \\
 &\hspace{25em} (\text{AI.1}) \\
 \sigma^{(1)}(r) &= \sqrt{2\pi} e^{-\frac{i\pi}{3}} \left(\frac{\zeta_\beta^{1/4}}{\lambda_\beta^{1/2}} \right) \text{Ai}(-e^{\frac{2i\pi}{3}} \zeta_\beta) \\
 \sigma^{(2)}(r) &= \sqrt{2\pi} e^{\frac{i\pi}{3}} \left(\frac{\zeta_\beta^{1/4}}{\lambda_\beta^{1/2}} \right) \text{Ai}(-e^{-\frac{2i\pi}{3}} \zeta_\beta) \\
 \sigma^{(3)}(r) &= \sqrt{2\pi} \left(\frac{\zeta_\beta^{1/4}}{\lambda_\beta^{1/2}} \right) \text{Ai}(-\zeta_\beta)
 \end{aligned}$$

where

Ai is an Airy function and

$$\zeta_\alpha = (3/2\omega\tau_\alpha)^{2/3}$$

$$\zeta_\beta = (3/2\omega\tau_\beta)^{2/3}$$

$$\tau_\alpha = \int_{r_p}^r \lambda_\alpha dr$$

$$\tau_\beta = \int_{r_p}^r \lambda_\beta dr$$

$$\lambda_\alpha = \sqrt{1/\alpha^2 - p^2/r^2}$$

$$\lambda_\beta = \sqrt{1/\beta^2 - p^2/r^2}$$

α and β are the P and S velocity respectively at radius r , p is the ray parameter in a spherical Earth, and r_p is the turning point radius, i.e., that radius at which λ_α or λ_β vanishes. In each inhomogeneous layer, the velocity functions $\alpha(r)$ and $\beta(r)$ are assumed to be analytic and to possess only one turning point r_p in the domain of complex p used in synthesizing a seismogram. The Langer approximated wavefunctions can also be written in terms of Hankel functions of order $1/3$ (Richards, 1976; Doornbos, 1981).

The π wavefunctions are those for P waves; the σ wavefunctions are those for S waves. Several possible pairs of independent solutions may be chosen to define fundamental matrices, which can be used to solve problems in wave propagation in media consisting of a sequence of vertically

inhomogeneous layers. The pairs $(\pi^{(1)}, \pi^{(2)})$ and $(\sigma^{(1)}, \sigma^{(2)})$ correspond to up- (1) and down-going (2) waves. The pairs $(\pi^{(1)}, \pi^{(3)})$ and $(\sigma^{(1)}, \sigma^{(3)})$ correspond to up-going (1) and standing or evanescent waves (3). When the turning point radius r_p is greater than r , the wavefunctions $\pi^{(3)}$ and $\sigma^{(3)}$ are always exponentially decaying functions with decreasing radius r .

Vertical Slownesses

Implementation of the Langer approximation in problems in which elastic boundary conditions must to be satisfied at model discontinuities is simplified by the introduction of generalized cosines (Richards, 1976; Aki and Richards, 1980) or generalized vertical slowness functions, which are defined as follows

$$\begin{aligned}\dot{\xi} &= \frac{d\pi^{(1)}}{dr} / (i\omega\pi^{(1)}) \\ \dot{\xi} &= - \frac{d\pi^{(2)}}{dr} / (i\omega\pi^{(1)}) \\ \dot{\xi} &= - \frac{d\pi^{(3)}}{dr} / (i\omega\pi^{(3)})\end{aligned}\tag{AI.2}$$

$$\begin{aligned}\dot{\eta} &= \frac{d\sigma^{(1)}}{dr} / (i\omega\sigma^{(1)}) \\ \dot{\eta} &= - \frac{d\sigma^{(2)}}{dr} / (i\omega\sigma^{(1)}) \\ \dot{\eta} &= - \frac{d\sigma^{(3)}}{dr} / (i\omega\sigma^{(3)})\end{aligned}$$

The normalization of the vertical wavefunctions differs slightly from that given in Aki and Richards (1980) and has been chosen such that the following relations are satisfied

$$\dot{\xi}\pi^{(1)}\pi^{(2)} + \dot{\xi}\pi^{(2)}\pi^{(1)} = 1$$

$$\dot{\xi}\pi^{(1)}\pi^{(3)} + \bar{\xi}\pi^{(3)}\pi^{(1)} = 1 \quad (\text{AI.3})$$

$$\dot{\eta}\sigma^{(1)}\pi^{(2)} + \dot{\eta}\sigma^{(2)}\pi^{(1)} = 1$$

$$\dot{\eta}\sigma^{(1)}\pi^{(3)} + \dot{\eta}\sigma^{(3)}\pi^{(1)} = 1$$

These relations can be demonstrated by substituting the Langer approximation to the vertical slownesses and the Wronskian relations between the Airy functions having different arguments. Equations AI.3 are satisfied exactly when only the zero order terms in frequency are kept in the definitions of the vertical slownesses.

Branch Cuts and Complex p

The functions that define the generalized vertical wavefunctions and slownesses as well as the special function subroutines from which Airy functions or Hankel functions of order $1/3$ are commonly constructed contain branch cuts emanating from points in the complex p plane corresponding to ray parameters grazing the model discontinuities. Extreme care must be exercised both in the definition and the choosing of branch cuts appearing in all functions of variables raised to fractional powers. A subroutine for the Langer approximated wavefunctions and vertical slownesses has been used, in which the branch cuts of the vertical wavefunctions are defined as in Cormier (1976) and Cormier and Richards (1989). This wavefunction subroutine has been tested in a wide variety of problems involving both complex velocities and complex p . For examples, see Cormier and Richards, (1989).

Fundamental Matrices

Boundary conditions in an medium consisting of n inhomogeneous layers can be handled in the same manner as a medium consisting of homogeneous layers, but with the Langer approximation to the vertical wavefunctions and vertical slownesses substituting for exponential functions and cosines.

P-SV

As a function of radius r , the fundamental matrix for P-SV propagation and Rayleigh modes is taken to be than given in Cormier (1980):

$$F(r) = \sqrt{\frac{i}{\rho}} \begin{bmatrix} \dot{\xi}\pi^{(1)} & -\dot{\xi}\pi^{(2)} & p/r \sigma^{(1)} & p/r \sigma^{(2)} \\ -i p/r \pi^{(1)} & -i p/r \pi^{(2)} & i\dot{\eta}\sigma^{(1)} & -i\dot{\eta}\sigma^{(2)} \\ -iA\pi^{(1)} & -iA\pi^{(2)} & iB\dot{\eta}\sigma^{(1)} & -iB\dot{\eta}\sigma^{(2)} \\ B\dot{\xi}\pi^{(1)} & -B\dot{\xi}\pi^{(2)} & A\sigma^{(1)} & A\sigma^{(2)} \end{bmatrix} \quad (\text{AI.4})$$

$$F(r)^{-1} = \sqrt{\frac{i}{\rho}} \begin{bmatrix} iA\pi^{(2)} & B\dot{\xi}\pi^{(2)} & -\dot{\xi}\pi^{(2)} & -i p/r \pi^{(2)} \\ -iA\pi^{(1)} & B\dot{\xi}\pi^{(1)} & -\dot{\xi}\pi^{(1)} & i p/r \pi^{(1)} \\ -iB\dot{\eta}\sigma^{(2)} & A\sigma^{(2)} & -p/r \sigma^{(2)} & i\dot{\eta}\sigma^{(2)} \\ -iB\dot{\eta}\sigma^{(1)} & -A\sigma^{(1)} & p/r \sigma^{(1)} & i\dot{\eta}\sigma^{(1)} \end{bmatrix}$$

The fundamental matrix may alternatively be defined using the wavefunction pairs $(\pi^{(1)}, \pi^{(3)})$ and $(\sigma^{(1)}, \sigma^{(2)})$ (Cormier, 1980). This fundamental matrix has exactly the same form as AI.4, but with (3) replacing the (2) superscripted wavefunctions and the ` accent replacing the ` in the

vertical slownesses. In all calculations, the (3) superscripted wavefunctions are substituted for the (2) superscripted (down-going) wavefunctions in the p domains in which exponentially decaying and growing vertical wavefunctions exist. With a few simple modifications described by Doornbos (1981), the fundamental matrix defined in AI.4 can be applied to layers having a negative as well as a positive gradient with depth.

Fundamental Matrix for SH Propagation

The SH fundamental matrix and its inverse are

$$F(r) = \sqrt{i} \begin{bmatrix} \mu^{-1/2} \sigma^{(1)} & \mu^{-1/2} \sigma^{(2)} \\ i \mu^{1/2} \dot{\eta} \sigma^{(1)} & -i \mu^{1/2} \sigma^{(2)} \end{bmatrix} \quad (AI.5)$$

$$F(r)^{-1} = \sqrt{i} \begin{bmatrix} -i \mu^{1/2} \dot{\eta} \sigma^{(2)} & -\mu^{-1/2} \sigma^{(2)} \\ -i \mu^{1/2} \dot{\eta} \sigma^{(1)} & \mu^{-1/2} \sigma^{(2)} \end{bmatrix}$$

Model Parameterization

Since the Langer approximation allows layers to be vertically inhomogeneous, the effects of Earth curvature are built into the model parameterization. All formulae are evaluated using velocities and densities given as functions of radius, r , from the Earth's center. In each inhomogeneous layer, the velocities are specified by analytic functions, which have only one turning point solution in the p domain of interest. Layer boundaries are introduced and boundary conditions are evaluated at discontinuities in velocity derivatives as well as first order discontinuities.

To provide analytic forms for the delay time functions τ_α and τ_β , each inhomogeneous layer is parameterized by making the flattened velocity be a linear function in the flattened depth coordinate, z . The usual (Müller, 1971) mapping between the flattened velocity function $v_f(z)$ and the true velocity function $v(r)$ is assumed :

$$v(r) = r v_f(z)/R_e$$

where

$$z_n^- = R_e \log(r_c/R_e)$$

where R_e is the radius of the Earth.

The flattened velocity function v_f is assumed to be a linear function in flattened depth, computed from the values of v_f at flattened depths z_n^- and z_{n-1}^+ corresponding to radii r_n^- and r_{n-1}^+ , bounding the top and bottom, respectively of vertically inhomogeneous layer n . The analytic form of the delay time function $\tau(r)$ becomes

$$\tau(r) = \frac{z_n^+ - z_n^-}{v_f(z_n^+) - v_f(z_n^-)} \left\{ \sqrt{R_e^2/p^2 - v_f^2} - R_e/p \left[\ln \left(\frac{R_e/p + \sqrt{R_e^2/p^2 - v_f^2}}{v_f} \right) \right] \right\} \quad (\text{A1.6})$$

This parameterization is adequate in representing thick regions of the crust and uppermost mantle, in which velocity gradients are nearly constant or slowly varying. Usually less than ten inhomogeneous layers are all that are needed to describe models having several first order discontinuities and/or discontinuities in gradient. Alternative model parameterizations, which give an analytic form of τ , are discussed by Cormier (1980), Červený and Jansky (1983), and Cormier and Richards (1989).

APPENDIX II – Mode Amplitudes and Eigenfunctions

Rayleigh Modes

The summation of locked Rayleigh modes requires the calculation of an antisymmetric Y matrix having five independent elements.

The Y Matrix

At the radius r_c at the top of the capping layer, starting values of the Y matrix are taken to be

$$Y_{12} = -A_c^2 - B_c^2 \lambda_{\alpha_c} \lambda_{\beta_c}$$

$$Y_{13} = -A_c p/r_c - B_c \lambda_{\alpha_c} \lambda_{\beta_c}$$

$$Y_{14} = -i \rho_c \lambda_{\beta_c} \quad (\text{AII.1})$$

$$Y_{23} = i \rho_c \lambda_{\alpha_c}$$

$$Y_{34} = -\lambda_{\beta_c} \lambda_{\alpha_c} - p^2/r_c^2$$

where $i = \sqrt{-1}$, and

$$\lambda_{\beta_c} = i \sqrt{p^2/r_c^2 - 1/\beta_c^2}$$

$$\lambda_{\alpha_c} = i \sqrt{p^2/r_c^2 - 1/\alpha_c^2}$$

$$A_c = 2p^2/r_c^2 \mu_c - \rho_c$$

$$B_c = 2 p^2/r_c^2 \mu_c$$

and μ_c , ρ_c , α_c , β_c are the shear modulus, density, P velocity, and S velocity, respectively, of the high velocity capping layer.

At any radius r , Y can be computed from the product

$$Y(r) = K^T(r, r_n^+) Y(r_n^-) K(r, r_n^+) \quad (\text{AII.2})$$

where K is a P-SV propagator matrix equal to a product of intralayer propagator matrices for each layer, m , $m+1$, etc.

$$K = K_m(r, r_m^+) K_{m+1}(r_m^-, r_{m+1}^+) \cdots K_n(r_{n-1}^-, r_n^+) \quad (\text{AII.3})$$

Layers are separated by boundaries at which velocities and/or densities have either first or second order discontinuities. Within each layer, the velocity functions are continuous, analytic functions. Each interlayer propagator matrix, K_m is constructed from the zeroth order term in frequency of the uniform asymptotic approximation to the fundamental matrix F of the inhomogeneous layer. Since the uniform asymptotic approximation of Langer is assumed, the velocity functions within each layer must have no more than one turning point for each ray parameter, p . With this restriction, computations can still be conducted in a complicated model having one or more low velocity zones, as long as this model is built from "layers" in which the analytic functions for P and S velocity have only a single turning point for each p .

The intralayer propagator is defined by

$$K_m(r_m^-, r_{m+1}^+) = F(r_m^-) F^{-1}(r_{m+1}^+) \quad (\text{AII.4})$$

Substituting in equation AII.2 the forms for the fundamental matrix and its inverse from equation AI.4, and simplifying the resulting expression gives recursion relations as follows for the

upward propagation of Y matrix elements:

$$\begin{aligned}
Y_{12}(r_n^-) &= \sum_{k=1}^4 {}_k d_1(r_n^-) {}_k W_n {}_k G_n - 2 A(r_{n-1}^+) B(r_{n-1}^+) {}_0 W_n {}_0 G_n \\
Y_{13}(r_n^-) &= - \sum_{k=1}^4 {}_k d_2(r_n^-) [A(r_{n-1}^+) B(r_{n-1}^+) - p/r_{n-1}^+ B(r_{n-1}^+)] {}_k W_n {}_k G_n \\
Y_{14}(r_n^{-1}) &= - \sum_{k=1}^4 {}_k d_3(r_n^{-1}) {}_k W_n {}_k G_n \\
Y_{23}(r_n^{-1}) &= - \sum_{k=1}^4 {}_k d_4(r_n^{-1}) {}_k W_n {}_k G_n \\
Y_{34}(r_n^-) &= - \sum_{k=1}^4 {}_k d_5(r_n^{-1}) {}_k W_n {}_k G_n + 2 p/r_{n-1}^+ {}_0 W_n {}_0 G_n
\end{aligned} \tag{AII.5}$$

where the quantities ${}_k d_l(z)$, ${}_k W_n$, ${}_k G_n$ are defined as follows:

$$\begin{aligned}
{}_k d_1(r) &= -A^2(r) - B^2(r) {}_k \lambda_\alpha(r) {}_k \lambda_\beta \\
{}_k d_2(r) &= A(r) p/r + B(z) {}_k \lambda_\alpha(r) {}_k \lambda_\beta(r) \\
{}_k d_3(r) &= i\rho(r) {}_k \lambda_\beta(r) \\
{}_k d_4(r) &= -i\rho(r) {}_k \lambda_\alpha(r) \\
{}_k d_5(r) &= {}_k \lambda_\beta(r) {}_k \lambda_\alpha(r) + (p/r)^2 \\
{}_k W_n &= -{}_k d_1(r_{n-1}^+) Y_{34}(r_{n-1}^-) + 2{}_k d_2(r_{n-1}^+) Y_{13}(r_{n-1}^-) + {}_k d_3(r_{n-1}^+) Y_{14}(r_{n-1}^-) \\
&\quad + {}_k d_4(r_{n-1}^+) Y_{23}(r_{n-1}^-) + {}_k d_5(r_{n-1}^+) Y_{12}(r_{n-1}^-)
\end{aligned} \tag{AII.6}$$

for $k \neq 0$ and

$$\begin{aligned}
{}_0 W_n &= p/r_n^+ Y_{12}(r_{n-1}^-) + [A(r_{n-1}^+) + p/r_{n-1}^+ B(r_{n-1}^+)] Y_{13}(r_{n-1}^-) \\
&\quad - A(r_{n-1}^+) B(r_{n-1}^+) Y_{34}(r_{n-1}^-)
\end{aligned} \tag{AII.7}$$

$$\begin{aligned}
{}_0G_n &= 4 \frac{r_n^-/r_{n-1}^+}{\sqrt{2\rho(r_n^-)\rho(r_{n-1}^+)}} \\
{}_1G_n &= \pi^{(2)}(r_n^-) \sigma^{(2)}(r_n^-) \pi^{(1)}(r_{n-1}^+) \sigma^{(1)}(r_{n-1}^+) \frac{r_n^-/r_{n-1}^+}{\sqrt{2\rho(r_n^-)\rho(r_{n-1}^+)}} \\
{}_2G_n &= -\pi^{(2)}(r_n^-) \sigma^{(1)}(r_n^-) \pi^{(1)}(r_{n-1}^+) \sigma^{(2)}(r_{n-1}^+) \frac{r_n^-/r_{n-1}^+}{\sqrt{2\rho(r_n^-)\rho(r_{n-1}^+)}} \\
{}_3G_n &= -\pi^{(1)}(r_n^-) \sigma^{(2)}(r_n^-) \pi^{(2)}(r_{n-1}^+) \sigma^{(1)}(r_{n-1}^+) \frac{r_n^-/r_{n-1}^+}{\sqrt{2\rho(r_n^-)\rho(r_{n-1}^+)}} \\
{}_4G_n &= \pi^{(1)}(r_n^-) \sigma^{(1)}(r_n^-) \pi^{(2)}(r_{n-1}^+) \sigma^{(2)}(r_{n-1}^+) \frac{r_n^-/r_{n-1}^+}{\sqrt{2\rho(r_n^-)\rho(r_{n-1}^+)}}
\end{aligned} \tag{AII.9}$$

${}_k\lambda_\alpha$ and ${}_k\lambda_\beta$ denote the following at boundaries r_n^- and r_n^+ :

$$\begin{aligned}
{}_1\lambda_\alpha(r_n^-) &= \dot{\xi}(r_n^-) \\
{}_1\lambda_\alpha(r_{n-1}^+) &= \dot{\xi}(r_{n-1}^+) \\
{}_1\lambda_\beta(r_n^-) &= \dot{\eta}(r_n^-) \\
{}_1\lambda_\beta(r_{n-1}^+) &= \dot{\eta}(r_{n-1}^+) \\
{}_2\lambda_\alpha(r_n^-) &= \dot{\xi}(r_n^{-1}) \\
{}_2\lambda_\alpha(r_{n-1}^+) &= \dot{\xi}(r_{n-1}^+) \\
{}_2\lambda_\beta(r_n^-) &= -\dot{\eta}(r_n^{-1}) \\
{}_2\lambda_\beta(r_{n-1}^+) &= -\dot{\eta}(r_{n-1}^+) \\
{}_3\lambda_\alpha(r_n^-) &= -\dot{\xi}(r_n^-) \\
{}_3\lambda_\alpha(r_{n-1}^+) &= -\dot{\xi}(r_{n-1}^+) \\
{}_3\lambda_\beta(r_n^-) &= \dot{\eta}(r_n^-) \\
{}_3\lambda_\beta(r_{n-1}^+) &= \dot{\eta}(r_{n-1}^+) \\
{}_4\lambda_\alpha(r_n^-) &= -\dot{\xi}(r_n^-)
\end{aligned}$$

$$4\lambda_{\alpha}(r_{n-1}^{+}) = -\dot{\xi}(r_{n-1}^{+})$$

$$4\lambda_{\beta}(r_n^{-}) = -\dot{\eta}(r_n^{-})$$

$$4\lambda_{\beta}(r_{n-1}^{+}) = -\dot{\eta}(r_{n-1}^{+})$$

Layer Reduction

The first term ($k = 1$) in the summation in equation AII.5 is of the same form as the starting values Y matrix in the capping layer in regions of slowness in which the vertical wavefunctions behave exponentially. When this first term is exponentially larger by several orders of magnitude than the ($k = 2, 3, 4, 5$) terms, then the Y matrix calculation may be started at a higher layer, taking this higher layer as the capping layer. This procedure of layer reduction is analogous to that described in homogeneously layered models (Panza and Sudhadolc, 1987).

Eigenfunctions

Although propagation of the Y matrix elements has been shown to be numerically stable at arbitrarily high frequency (Abo-Zena 1979; Harvey, 1981), numerical problems in the calculation of the Rayleigh eigenfunctions reoccur if E is calculated by multiplying propagator matrices. One approach to this problem is to divide a layer into thin, pseudo layers, and rescale the propagator matrix after propagation through each thin layer. Better techniques, however, can be formulated, which do not require the introduction of additional pseudo layers.

One technique, described by Harvey (1985), expresses the eigenfunctions in terms of Y matrix elements by propagating the wavefield upward from the cap layer and downward from the free

surface. Thus, since the calculation of Y elements is numerically stable, so is the calculation of the E eigenfunctions. In this technique, eigenvalues can be normalized at the source depth, offering numerical advantages in the calculation of channel waves having vanishingly small energy outside of a waveguide.

The technique used here also does not require pseudo layering, but retains the standard normalization of the E_1 function to 1 at the free surface. The first step in this technique is to recognize that the stress eigenfunctions E_3 and E_4 can be calculated from the displacement eigenfunctions E_1 and E_2 by

$$E_3 = -Y_{14}/Y_{34} E_1 - Y_{24}/Y_{34} E_2 \quad (\text{AII.10})$$

$$E_4 = Y_{13}/Y_{34} E_1 + Y_{23}/Y_{34} E_2$$

Using these relations, the four equations that propagate the E vector,

$$E(r) = K(r, r_n) E(r_n) \quad (\text{AII.11})$$

can be rewritten as two equations that propagate E_1 and E_2 ,

$$\begin{bmatrix} E_1(r) \\ E_2(r) \end{bmatrix} = L(z, z_n) \begin{bmatrix} E_1(r_n) \\ E_2(r_n) \end{bmatrix} \quad (\text{AII.12})$$

and the two equations given in AII.10 between the displacement eigenfunctions and stress eigenfunctions.

A new 2x2 propagator matrix L is defined having components

$$L_{11} = K_{11} - K_{13} Y_{14}/Y_{34} + K_{14} Y_{13}/Y_{34}$$

$$L_{12} = K_{12} - K_{13} Y_{24}/Y_{34} + K_{14} Y_{23}/Y_{34}$$

(AII.13)

$$L_{21} = K_{21} - K_{23} Y_{14}/Y_{34} + K_{24} Y_{13}/Y_{34}$$

$$L_{22} = K_{22} + K_{23} Y_{24}/Y_{34} + K_{24} Y_{23}/Y_{34}$$

To ensure numerical precision in a machine calculation, the individual propagator elements as well as the recursion formulae in AII 5 for the Y matrix elements must be substituted into the definitions of the the L_{ij} elements in AII.13, a fraction formed with the common denominator of Y_{34} , and the numerator of the fraction simplified. When this simplification is done, it is seen that all numerator terms that potentially are of the largest exponential order cancel. Although many cancellations occur, the resulting expressions for the L_{ij} elements are still quite lengthy and are not given here.

Love Modes

D_1 and D_2

In this case, calculation of the dispersion function D_1 eigenfunction vector E can proceed by simple multiplication of propagator matrices without loss of numerical precision. The vector (D_1, D_2) in the notation of Harvey (1985) is equal to the vector E_{SH} in the notation of Cormier (1980). In the capping layer, (D_1, D_2) is simply equal to the first row of the inverse fundamental matrix

for SH waves. Any constant may be chosen to multiply the starting value of (D_1, D_2) , since this constant will cancel in the definition of eigenfunctions and in the ratio $\frac{Lk D_2(0)}{\partial D_1(0)/\partial k}$ appearing in the expression for the total response. Starting values of D_1 and D_2 at the top of the cap layer are thus taken as

$$D_1 = -i \rho_c \beta_c \lambda_{\beta_c} \quad (\text{AII.14})$$

$$D_2 = -1/\beta_c$$

D_1 and D_2 are propagated upward by multiplication of SH propagator matrices. Since (D_1, D_2) are related to the inverse fundamental matrix, one must right multiply the starting values by the SH propagator matrix.

$$\begin{bmatrix} D_1(r) \\ D_2(r) \end{bmatrix} = \begin{bmatrix} D_1(r_c) \\ D_2(r_c) \end{bmatrix} \mathbf{K}(r, r_c^+) \quad (\text{AII.15})$$

Eigenfunctions

Love wave eigenfunctions are defined by

$$E_1(r) = D_2(r)/D_2(R_e) \quad (\text{AII.16})$$

$$E_2(r) = D_1(r)/D_2(R_e)$$

In the residue calculation, scale factors can be applied in each layer and discarded during upward propagation. This is because all scale factors cancel when ratio $\frac{LkD_2(0)}{\partial D_1(0)/\partial k}$ is formed. In the eigenfunction calculation, the total scale factor of each D_i must be saved in order to properly describe regions of exponential decay of the eigenfunction. In the cases where E_1 and E_2 are exponentially small, the depth of the capping layer can be raised and calculations started at a shallower depth.

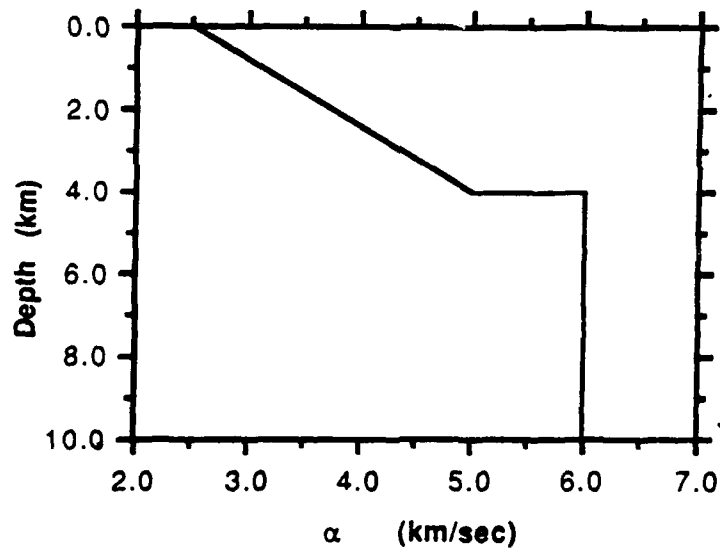
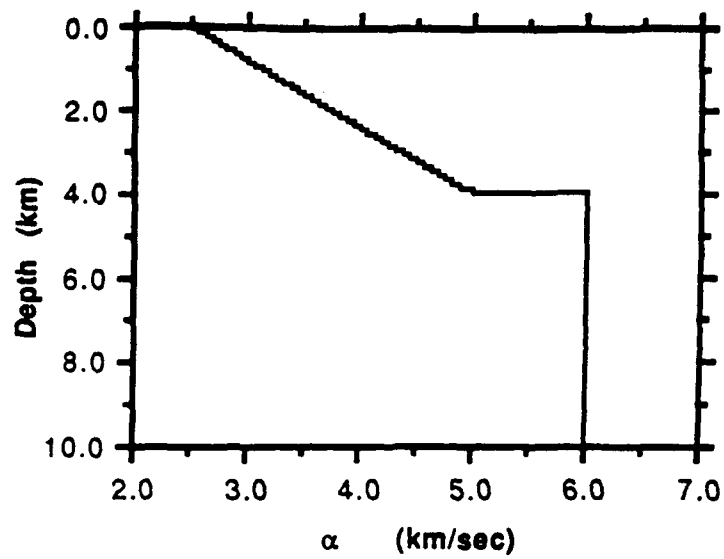


Figure 1: Discrete (above) and continuous (below) representations of a gradient in P velocity in a test model of the crust.

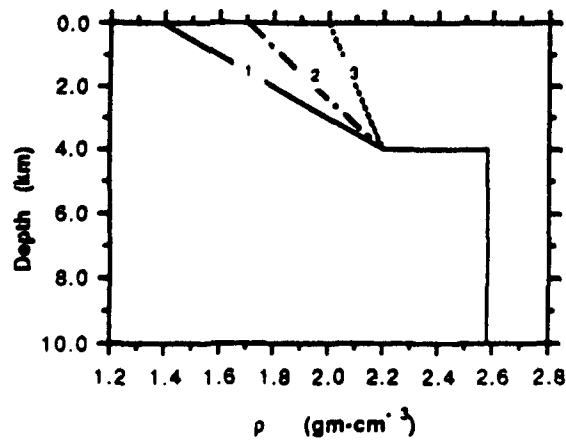
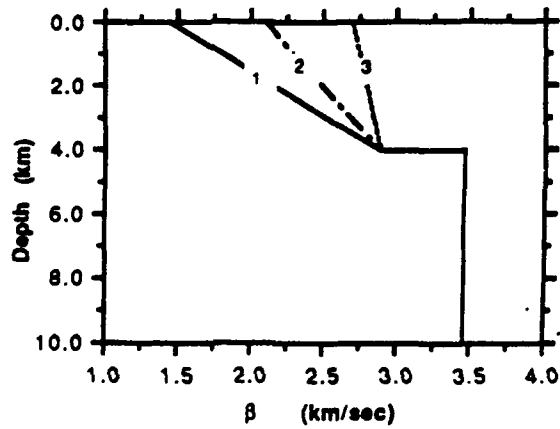
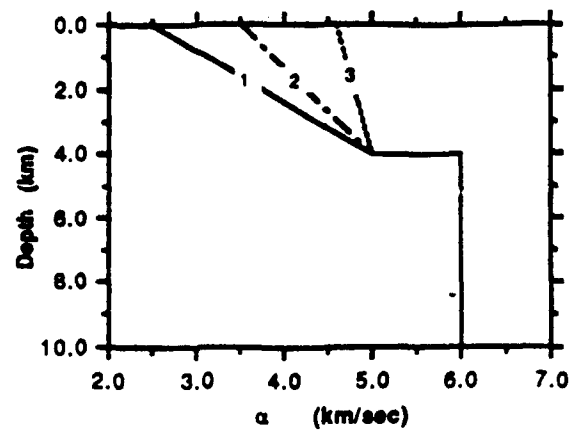


Figure 2: Test models having three different intensities of gradients in an inhomogeneous layer overlaying a homogeneous halfspace. Model 1 is the test model of Spudich and Ascher (1983)

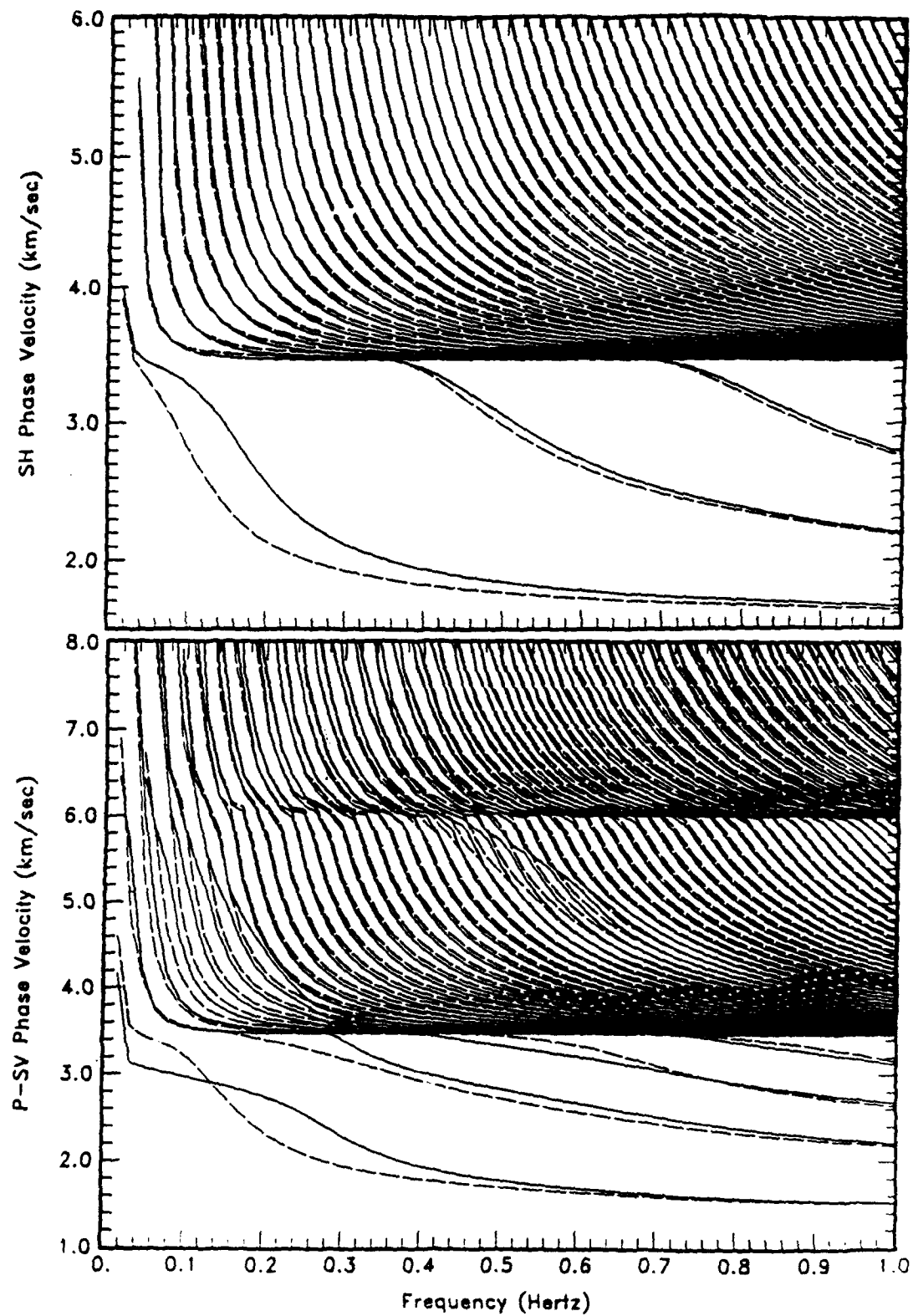


Figure 3: (a) Love and (b) Rayleigh mode dispersion curves calculated in Model 1 using a thin layered representation of the gradient layer (solid) and the Langer approximation in a continuous representation of the gradient layer (dashed).

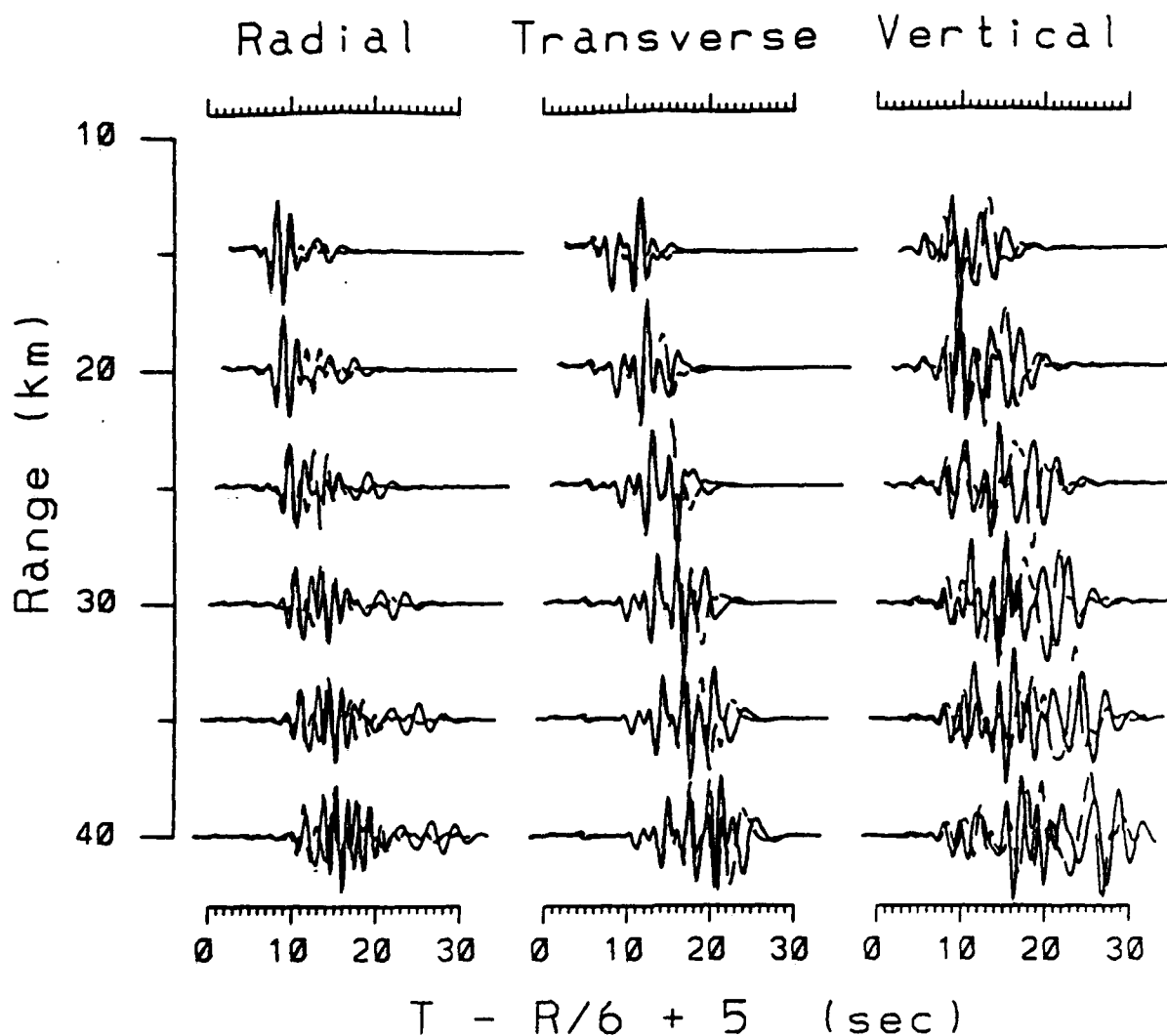


Figure 4: Comparison of synthetic seismograms calculated in Model 1 using a thin layered representation of the gradient layer (solid) and the Langer approximation in a continuous representation of the gradient layer (dashed). The source is a point double couple at 4.92 km. depth, corresponding to a vertically dipping strike slip fault, striking to the north, observed at receivers at 45° azimuth. A step function time dependence of the scalar moment is assumed. Shown are the three components of particle velocity. The effects of geometric spreading of body waves have been approximately removed by multiplying each seismogram by range.

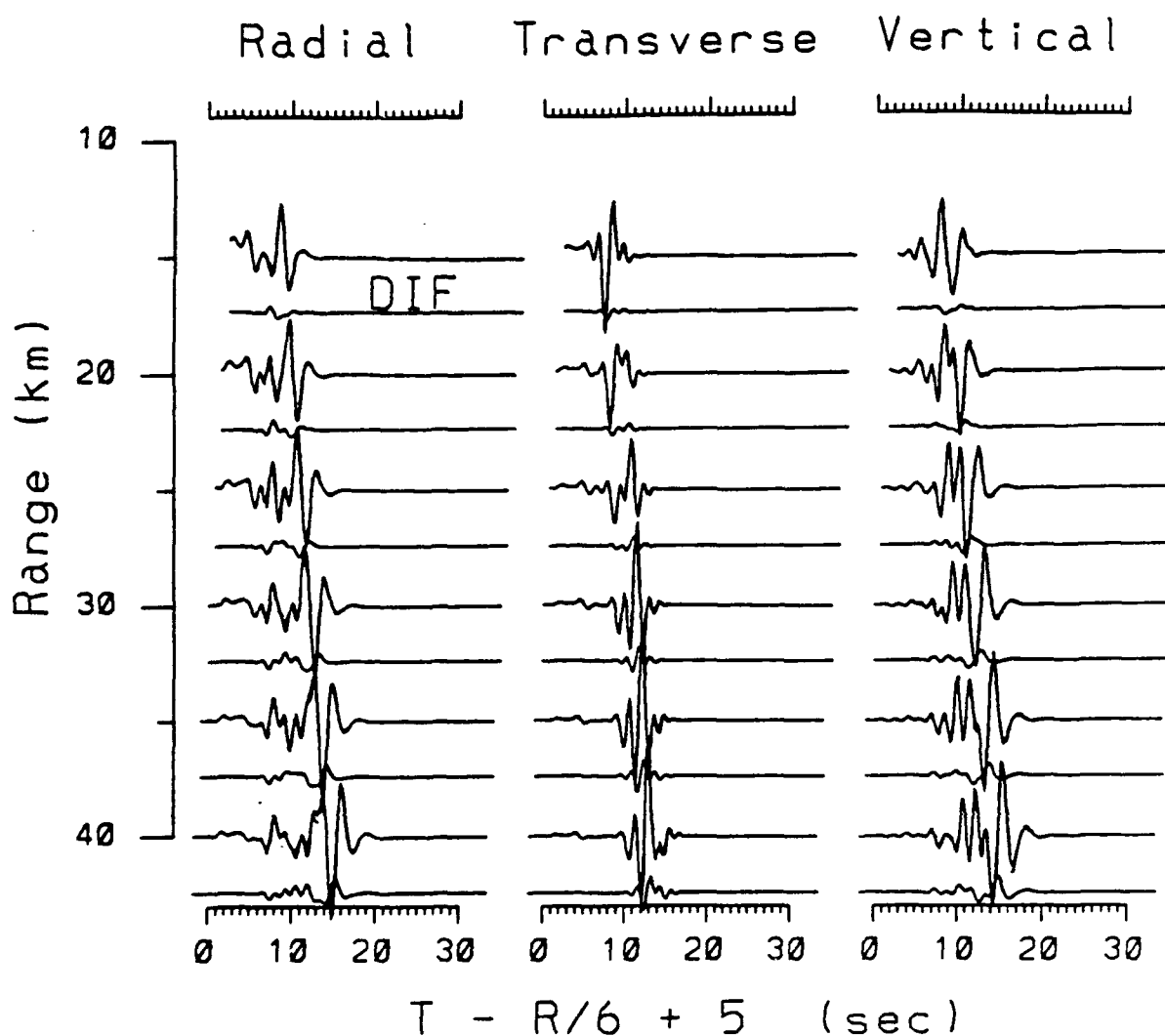


Figure 5: Comparison of synthetic seismograms calculated in Model 3 using a thin layered representation of the gradient layer and the Langer approximation in a continuous representation of the gradient layer. The result of the discrete method is shown at each range. The lower amplitude trace labeled DIF is the difference between the seismograms calculated by the two different parameterizations, (D) discrete thin layered and (CL) continuous with the Langer approximation, i.e., $DIF(t) = S_D(t) - S_{CL}(t)$. An approximate correction for geometric spreading of body waves has been made.

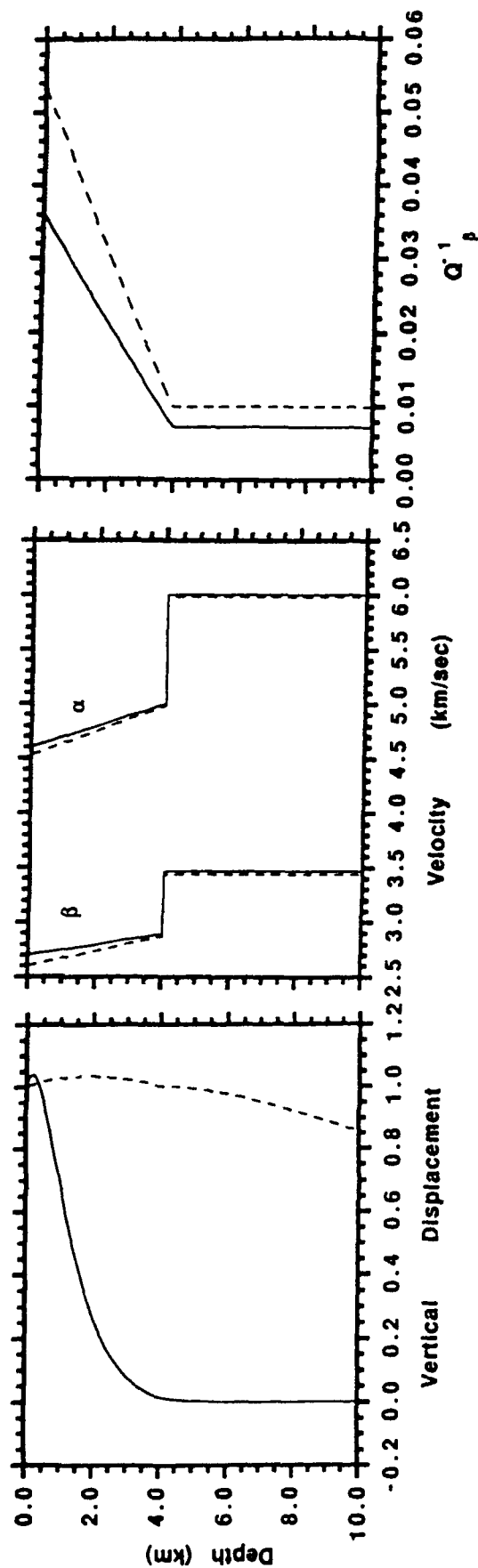


Figure 6: Seismograms for the fundamental Rayleigh mode were synthesized in a test anelastic model. (a) Left. Surface normalized displacement at 1 Hz. (solid) and 0.1 Hz. (dashed). (b) Middle. P and S velocity at 1 Hz. (solid) and 0.1 Hz. (dashed). (c) Right. Shear attenuation, Q_{β}^{-1} , at 1 Hz. (solid) and 0.1 Hz. (dashed).

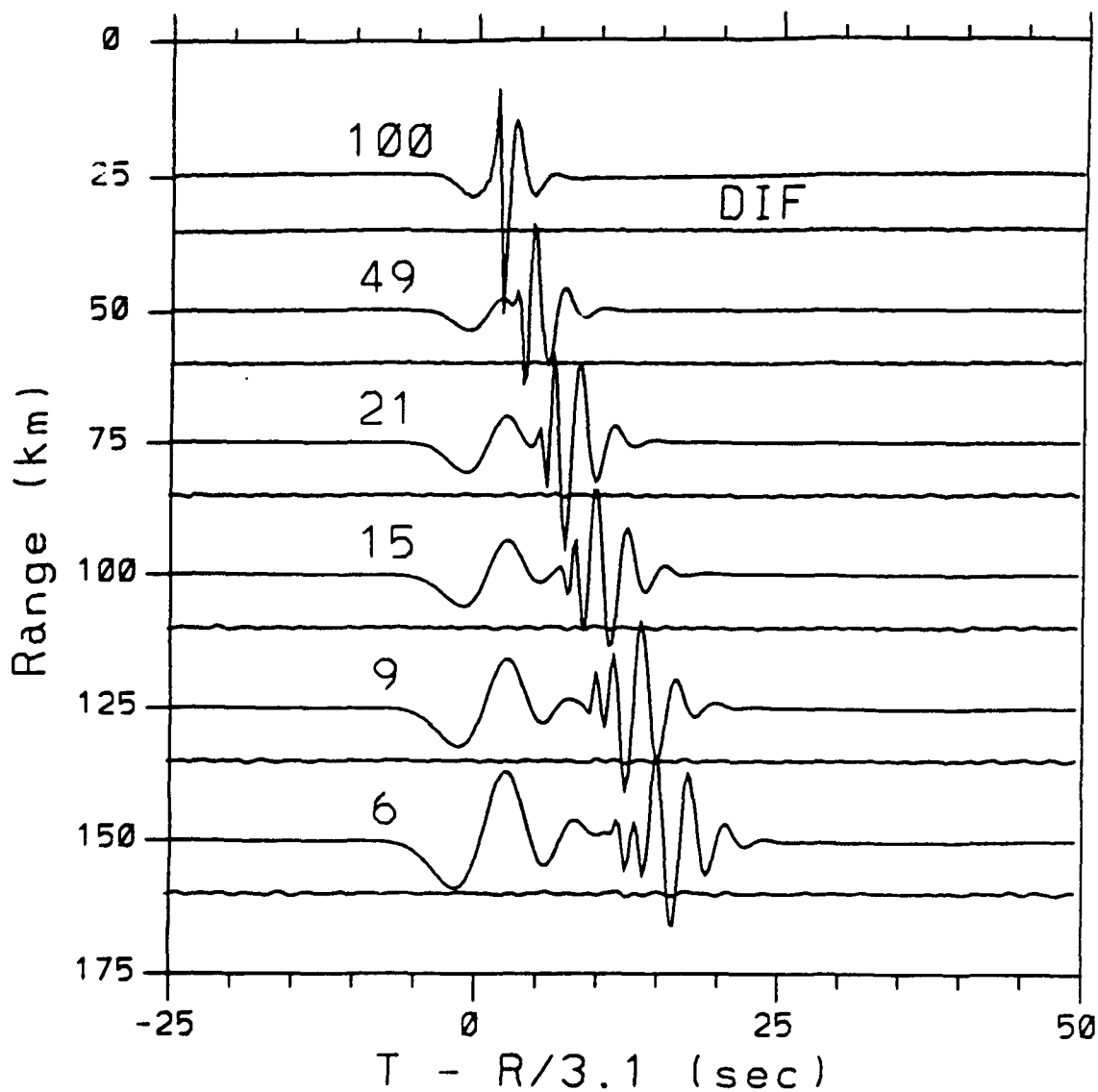


Figure 7: A comparison of the synthetic for the vertical component of the fundamental mode Rayleigh wave using perturbation theory and an exact, complex mode calculation. At each range, the results of the exact calculation are followed by the differential seismogram obtained by subtracting the seismogram calculated by perturbation theory from the seismogram calculated by complex modes and eigenfunctions. Each trace is normalized by its peak amplitude, indicated by the number to the left of each trace.

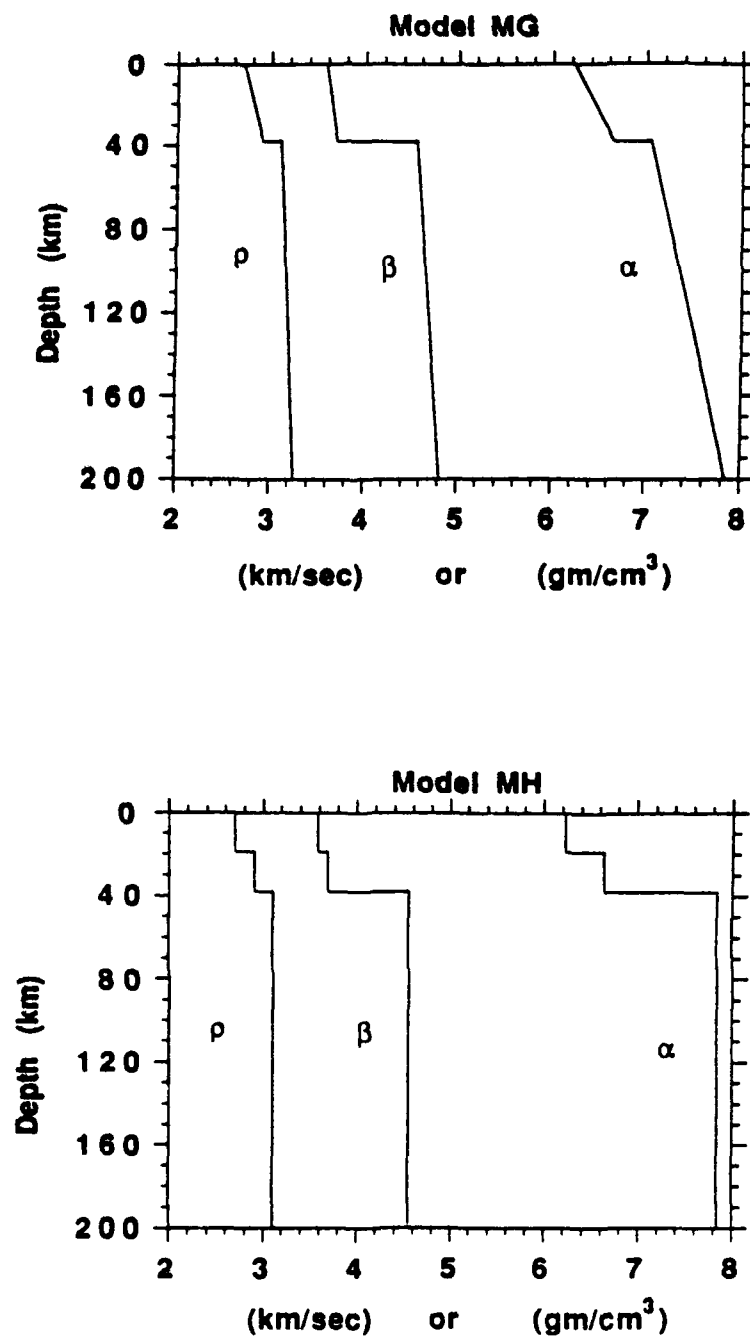


Figure 8: A simple crust and upper mantle model MH composed of two homogeneous crustal layers and overlaying a homogeneous mantle; and model MG having a single crustal gradient layer and mantle gradient layer.

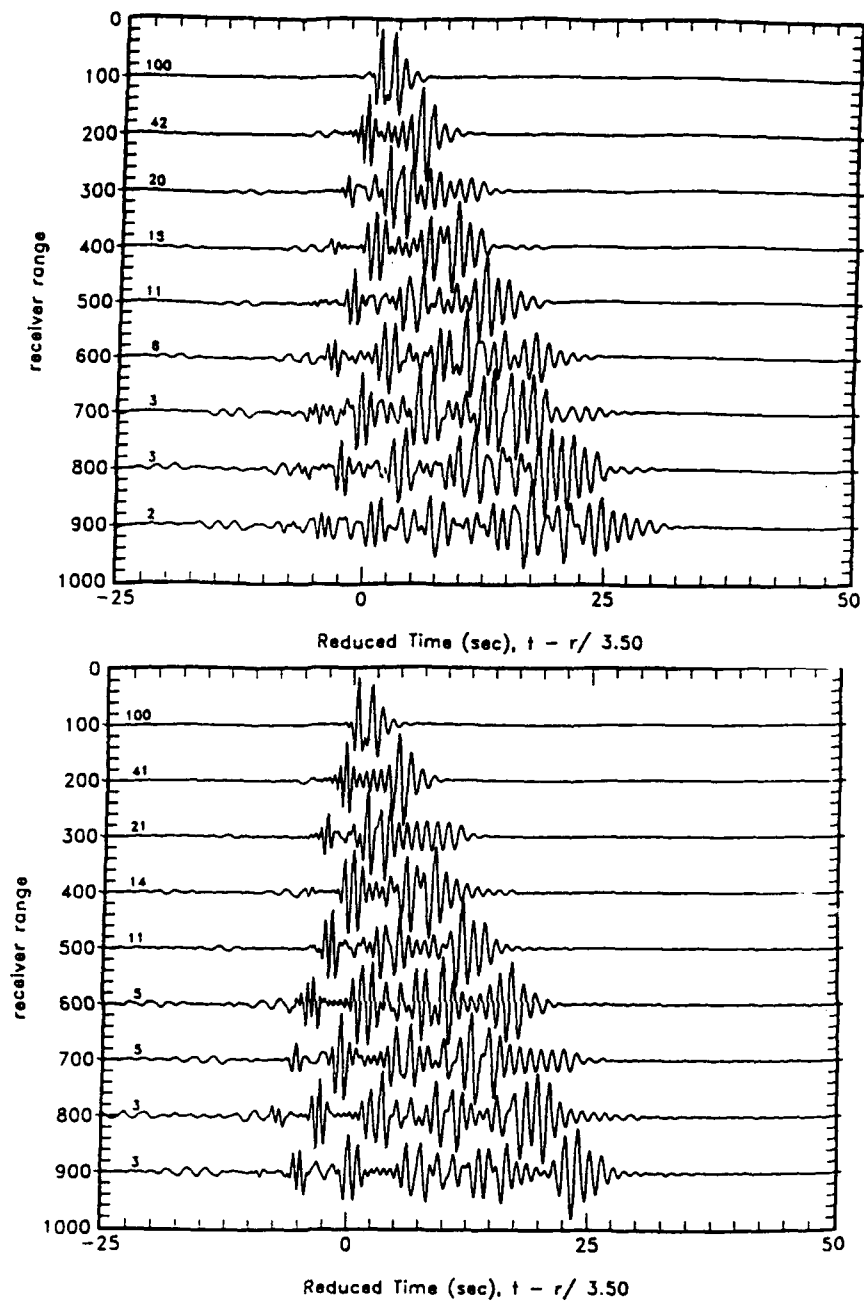


Figure 9: A comparison of synthetics in model MH (above) and MG (below) computed by the Langer-locked mode method, summing the first 10 Rayleigh modes. Shown is the vertical displacement for a double couple point source at 30 km depth. The orientation of the double couple corresponds to a vertically dipping strike slip fault, striking to the north, observed at an azimuth of 45° . A step function time dependence of the scalar moment is assumed, and the result has been convolved with a short period WWSSN instrument response.

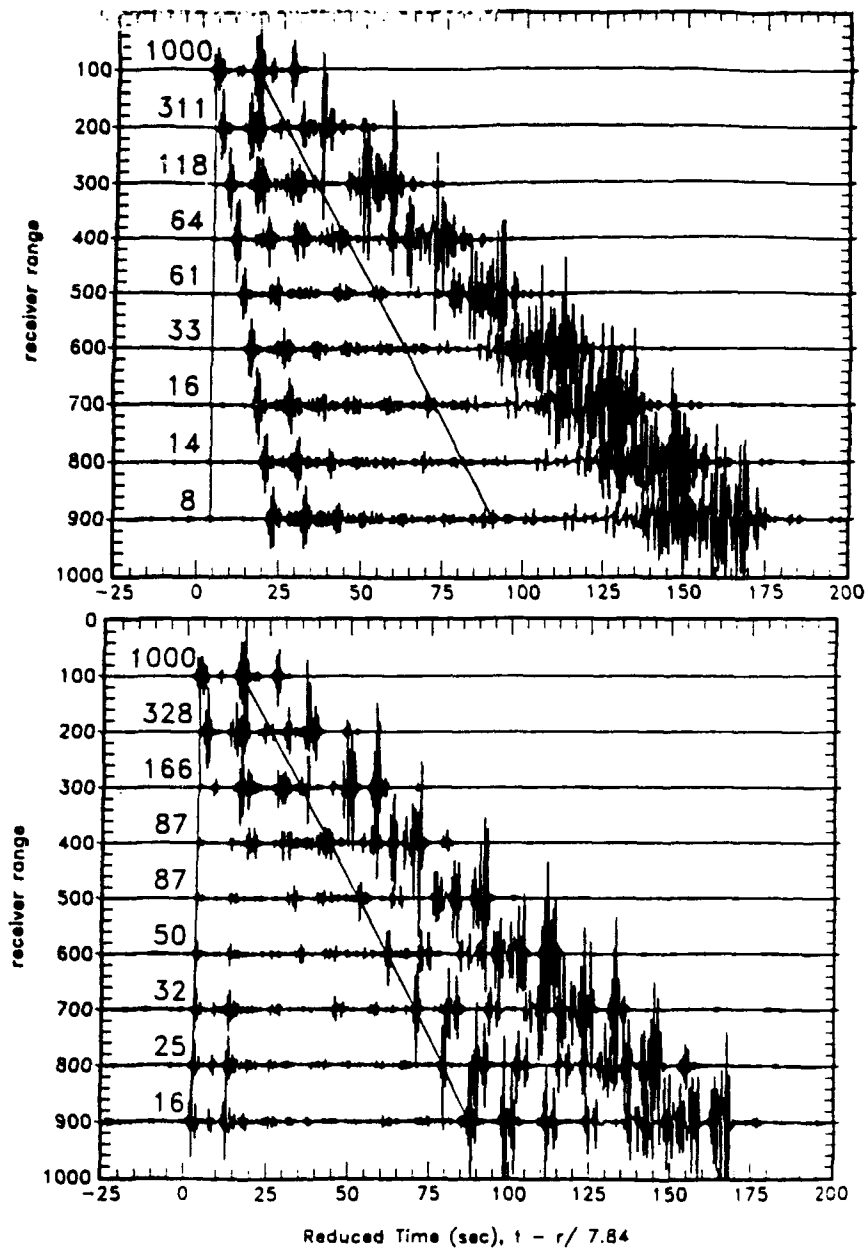


Figure 10: A comparison of synthetics in model MH (above) and MG (below) computed by the Langer-locked mode methods, summing all of the Rayleigh modes in a frequency band up to 2 Hz. Source, receivers, and instrument are described in figure 9.

CONTRACTORS (United States)

Prof. Thomas Ahrens
Seismological Lab, 252-21
Division of Geological & Planetary Sciences
California Institute of Technology
Pasadena, CA 91125

Prof. Charles B. Archambeau
CIRES
University of Colorado
Boulder, CO 80309

Dr. Thomas C. Bache, Jr.
Science Applications Int'l Corp.
10260 Campus Point Drive
San Diego, CA 92121 (2 copies)

Prof. Muawia Barazangi
Institute for the Study of the Continent
Cornell University
Ithaca, NY 14853

Dr. Douglas R. Baumgardt
ENSCO, Inc
5400 Port Royal Road
Springfield, VA 22151-2388

Prof. Jonathan Berger
IGPP, A-025
Scripps Institution of Oceanography
University of California, San Diego
La Jolla, CA 92093

Dr. Lawrence J. Burdick
Woodward-Clyde Consultants
566 El Dorado Street
Pasadena, CA 91109-3245

Dr. Karl Coyner
New England Research, Inc.
76 Olcott Drive
White River Junction, VT 05001

Prof. Vernon F. Cormier
Department of Geology & Geophysics
U-45, Room 207
The University of Connecticut
Storrs, CT 06268

Professor Anton W. Dainty
Earth Resources Laboratory
Massachusetts Institute of Technology
42 Carleton Street
Cambridge, MA 02142

Prof. Steven Day
Department of Geological Sciences
San Diego State University
San Diego, CA 92182

Dr. Zoltan A. Der
ENSCO, Inc.
5400 Port Royal Road
Springfield, VA 22151-2388

Prof. John Ferguson
Center for Lithospheric Studies
The University of Texas at Dallas
P.O. Box 830688
Richardson, TX 75083-0688

Prof. Stanley Flatte
Applied Sciences Building
University of California
Santa Cruz, CA 95064

Dr. Alexander Florence
SRI International
333 Ravenswood Avenue
Menlo Park, CA 94025-3493

Prof. Stephen Grand
University of Texas at Austin
Department of Geological Sciences
Austin, TX 78713-7909

Prof. Henry L. Gray
Vice Provost and Dean
Department of Statistical Sciences
Southern Methodist University
Dallas, TX 75275

Dr. Indra Gupta
Teledyne Geotech
314 Montgomery Street
Alexandria, VA 22314

Prof. David G. Harkrider
Seismological Laboratory
Division of Geological & Planetary Sciences
California Institute of Technology
Pasadena, CA 91125

Prof. Donald V. Helmberger
Seismological Laboratory
Division of Geological & Planetary Sciences
California Institute of Technology
Pasadena, CA 91125

Prof. Eugene Herrin
Institute for the Study of Earth and Man
Geophysical Laboratory
Southern Methodist University
Dallas, TX 75275

Prof. Robert B. Herrmann
Department of Earth & Atmospheric Sciences
St. Louis University
St. Louis, MO 63156

Prof. Bryan Isacks
Cornell University
Department of Geological Sciences
SNEE Hall
Ithaca, NY 14850

Dr. Rong-Song Jih
Teledyne Geotech
314 Montgomery Street
Alexandria, VA 22314

Prof. Lane R. Johnson
Seismographic Station
University of California
Berkeley, CA 94720

Prof. Alan Kafka
Department of Geology & Geophysics
Boston College
Chestnut Hill, MA 02167

Dr. Richard LaCoss
MIT-Lincoln Laboratory
M-200B
P. O. Box 73
Lexington, MA 02173-0073 (3 copies)

Prof. Fred K. Lamb
University of Illinois at Urbana-Champaign
Department of Physics
1110 West Green Street
Urbana, IL 61801

Prof. Charles A. Langston
Geosciences Department
403 Deike Building
The Pennsylvania State University
University Park, PA 16802

Prof. Thorne Lay
Institute of Tectonics
Earth Science Board
University of California, Santa Cruz
Santa Cruz, CA 95064

Prof. Arthur Lerner-Lam
Lamont-Doherty Geological Observatory
of Columbia University
Palisades, NY 10964

Dr. Christopher Lynnes
Teledyne Geotech
314 Montgomery Street
Alexandria, VA 22314

Prof. Peter Malin
University of California at Santa Barbara
Institute for Crustal Studies
Santa Barbara, CA 93106

Dr. Randolph Martin, III
New England Research, Inc.
76 Olcott Drive
White River Junction, VT 05001

Dr. Gary McCartor
Mission Research Corporation
735 State Street
P.O. Drawer 719
Santa Barbara, CA 93102 (2 copies)

Prof. Thomas V. McEvilly
Seismographic Station
University of California
Berkeley, CA 94720

Dr. Keith L. McLaughlin
S-CUBED
A Division of Maxwell Laboratory
P.O. Box 1620
La Jolla, CA 92038-1620

Prof. William Menke
Lamont-Doherty Geological Observatory
of Columbia University
Palisades, NY 10964

Stephen Miller
SRI International
333 Ravenswood Avenue
Box AF 116
Menlo Park, CA 94025-3493

Prof. Bernard Minster
IGPP, A-025
Scripps Institute of Oceanography
University of California, San Diego
La Jolla, CA 92093

Prof. Brian J. Mitchell
Department of Earth & Atmospheric Sciences
St. Louis University
St. Louis, MO 63156

Mr. Jack Murphy
S-CUBED, A Division of Maxwell Laboratory
11800 Sunrise Valley Drive
Suite 1212
Reston, VA 22091 (2 copies)

Dr. Bao Nguyen
GL/LWH
Hanscom AFB, MA 01731-5000

Prof. John A. Orcutt
IGPP, A-025
Scripps Institute of Oceanography
University of California, San Diego
La Jolla, CA 92093

Prof. Keith Priestley
University of Cambridge
Bullard Labs, Dept. of Earth Sciences
Madingley Rise, Madingley Rd.
Cambridge CB3 0EZ, ENGLAND

Prof. Paul G. Richards
L-210
Lawrence Livermore National Laboratory
Livermore, CA 94550

Dr. Wilmer Rivers
Teledyne Geotech
314 Montgomery Street
Alexandria, VA 22314

Prof. Charles G. Sammis
Center for Earth Sciences
University of Southern California
University Park
Los Angeles, CA 90089-0741

Prof. Christopher H. Scholz
Lamont-Doherty Geological Observatory
of Columbia University
Palisades, NY 10964

Thomas J. Sereno, Jr.
Science Application Int'l Corp.
10260 Campus Point Drive
San Diego, CA 92121

Prof. David G. Simpson
Lamont-Doherty Geological Observatory
of Columbia University
Palisades, NY 10964

Dr. Jeffrey Stevens
S-CUBED
A Division of Maxwell Laboratory
P.O. Box 1620
La Jolla, CA 92038-1620

Prof. Brian Stump
Institute for the Study of Earth & Man
Geophysical Laboratory
Southern Methodist University
Dallas, TX 75275

Prof. Jeremiah Sullivan
University of Illinois at Urbana-Champaign
Department of Physics
1110 West Green Street
Urbana, IL 61801

Prof. Clifford Thurber
University of Wisconsin-Madison
Department of Geology & Geophysics
1215 West Dayton Street
Madison, WI 53706

Prof. M. Nafi Toksoz
Earth Resources Lab
Massachusetts Institute of Technology
42 Carleton Street
Cambridge, MA 02142

Prof. John E. Vidale
University of California at Santa Cruz
Seismological Laboratory
Santa Cruz, CA 95064

Prof. Terry C. Wallace
Department of Geosciences
Building #77
University of Arizona
Tucson, AZ 85721

Dr. Raymond Willeman
GL/LWH
Hanscom AFB, MA 01731-5000

Dr. Lorraine Wolf
GL/LWH
Hanscom AFB, MA 01731-5000

OTHERS (United States)

Dr. Monem Abdel-Gawad
Rockwell International Science Center
1049 Camino Dos Rios
Thousand Oaks, CA 91360

Prof. Keiiti Aki
Center for Earth Sciences
University of Southern California
University Park
Los Angeles, CA 90089-0741

Prof. Shelton S. Alexander
Geosciences Department
403 Deike Building
The Pennsylvania State University
University Park, PA 16802

Dr. Kenneth Anderson
BBNSTC
Mail Stop 14/1B
Cambridge, MA 02238

Dr. Ralph Archuleta
Department of Geological Sciences
University of California at Santa Barbara
Santa Barbara, CA 93102

J. Barker
Department of Geological Sciences
State University of New York
at Binghamton
Vestal, NY 13901

Dr. T.J. Bennett
S-CUBED
A Division of Maxwell Laboratory
11800 Sunrise Valley Drive, Suite 1212
Reston, VA 22091

Mr. William J. Best
907 Westwood Drive
Vienna, VA 22180

Dr. N. Biswas
Geophysical Institute
University of Alaska
Fairbanks, AK 99701

Dr. G.A. Bollinger
Department of Geological Sciences
Virginia Polytechnical Institute
21044 Derring Hall
Blacksburg, VA 24061

Dr. Stephen Bratt
Center for Seismic Studies
1300 North 17th Street
Suite 1450
Arlington, VA 22209

Michael Browne
Teledyne Geotech
3401 Shiloh Road
Garland, TX 75041

Mr. Roy Burger
1221 Serry Road
Schenectady, NY 12309

Dr. Robert Burrige
Schlumberger-Doll Research Center
Old Quarry Road
Ridgefield, CT 06877

Dr. Jerry Carter
Rondout Associates
P.O. Box 224
Stone Ridge, NY 12484

Dr. W. Winston Chan
Teledyne Geotech
314 Montgomery Street
Alexandria, VA 22314-1581

Dr. Theodore Cherry
Science Horizons, Inc.
710 Encinitas Blvd., Suite 200
Encinitas, CA 92024 (2 copies)

Prof. Jon F. Claerbout
Department of Geophysics
Stanford University
Stanford, CA 94305

Prof. Robert W. Clayton
Seismological Laboratory
Division of Geological & Planetary Sciences
California Institute of Technology
Pasadena, CA 91125

Prof. F. A. Dahlen
Geological and Geophysical Sciences
Princeton University
Princeton, NJ 08544-0636

Prof. Adam Dziewonski
Hoffman Laboratory
Harvard University
20 Oxford St
Cambridge, MA 02138

Prof. John Ebel
Department of Geology & Geophysics
Boston College
Chestnut Hill, MA 02167

Eric Fielding
SNEE Hall
INSTOC
Cornell University
Ithaca, NY 14853

Prof. Donald Forsyth
Department of Geological Sciences
Brown University
Providence, RI 02912

Dr. Cliff Frolich
Institute of Geophysics
8701 North Mopac
Austin, TX 78759

Dr. Anthony Gangi
Texas A&M University
Department of Geophysics
College Station, TX 77843

Dr. Freeman Gilbert
Inst. of Geophysics & Planetary Physics
University of California, San Diego
P.O. Box 109
La Jolla, CA 92037

Mr. Edward Giller
Pacific Sierra Research Corp.
1401 Wilson Boulevard
Arlington, VA 22209

Dr. Jeffrey W. Given
SAIC
10260 Campus Point Drive
San Diego, CA 92121

Prof. Roy Greenfield
Geosciences Department
403 Deike Building
The Pennsylvania State University
University Park, PA 16802

Dan N. Hagedorn
Battelle
Pacific Northwest Laboratories
Battelle Boulevard
Richland, WA 99352

Kevin Hutchenson
Department of Earth Sciences
St. Louis University
3507 Laclede
St. Louis, MO 63103

Prof. Thomas H. Jordan
Department of Earth, Atmospheric
and Planetary Sciences
Massachusetts Institute of Technology
Cambridge, MA 02139

Robert C. Kemerait
ENSCO, Inc.
445 Pineda Court
Melbourne, FL 32940

William Kikendall
Teledyne Geotech
3401 Shiloh Road
Garland, TX 75041

Prof. Leon Knopoff
University of California
Institute of Geophysics & Planetary Physics
Los Angeles, CA 90024

Prof. L. Timothy Long
School of Geophysical Sciences
Georgia Institute of Technology
Atlanta, GA 30332

Prof. Art McGarr
Mail Stop 977
Geological Survey
345 Middlefield Rd.
Menlo Park, CA 94025

Dr. George Mellman
Sierra Geophysics
11255 Kirkland Way
Kirkland, WA 98033

Prof. John Nabelek
College of Oceanography
Oregon State University
Corvallis, OR 97331

Prof. Geza Nagy
University of California, San Diego
Department of Ames, M.S. B-010
La Jolla, CA 92093

Prof. Amos Nur
Department of Geophysics
Stanford University
Stanford, CA 94305

Prof. Jack Oliver
Department of Geology
Cornell University
Ithaca, NY 14850

Prof. Robert Phinney
Geological & Geophysical Sciences
Princeton University
Princeton, NJ 08544-0636

Dr. Paul Pomeroy
Rondout Associates
P.O. Box 224
Stone Ridge, NY 12484

Dr. Jay Pulli
RADIX System, Inc.
2 Taft Court, Suite 203
Rockville, MD 20850

Dr. Norton Rimer
S-CUBED
A Division of Maxwell Laboratory
P.O. Box 1620
La Jolla, CA 92038-1620

Prof. Larry J. Ruff
Department of Geological Sciences
1006 C.C. Little Building
University of Michigan
Ann Arbor, MI 48109-1063

Dr. Richard Sailor
TASC Inc.
55 Walkers Brook Drive
Reading, MA 01867

John Sherwin
Teledyne Geotech
3401 Shiloh Road
Garland, TX 75041

Prof. Robert Smith
Department of Geophysics
University of Utah
1400 East 2nd South
Salt Lake City, UT 84112

Dr. Stewart W. Smith
Geophysics AK-50
University of Washington
Seattle, WA 98195

Dr. George Sutton
Rondout Associates
P.O. Box 224
Stone Ridge, NY 12484

Prof. L. Sykes
Lamont-Doherty Geological Observatory
of Columbia University
Palisades, NY 10964

Prof. Pradeep Talwani
Department of Geological Sciences
University of South Carolina
Columbia, SC 29208

Prof. Ta-liang Teng
Center for Earth Sciences
University of Southern California
University Park
Los Angeles, CA 90089-0741

Dr. R.B. Tittmann
Rockwell International Science Center
1049 Camino Dos Rios
P.O. Box 1085
Thousand Oaks, CA 91360

Dr. Gregory van der Vink
IRIS, Inc.
1616 North Fort Myer Drive
Suite 1440
Arlington, VA 22209

Professor Daniel Walker
University of Hawaii
Institute of Geophysics
Honolulu, HI 96822

William R. Walter
Seismological Laboratory
University of Nevada
Reno, NV 89557

Dr. Gregory Wojcik
Weidlinger Associates
4410 El Camino Real
Suite 110
Los Altos, CA 94022

Prof. John H. Woodhouse
Hoffman Laboratory
Harvard University
20 Oxford St.
Cambridge, MA 02138

Prof. Francis T. Wu
Department of Geological Sciences
State University of New York
at Binghamton
Vestal, NY 13901

Dr. Gregory B. Young
ENSCO, Inc.
5400 Port Royal Road
Springfield, VA 22151-2388

GOVERNMENT

Dr. Ralph Alewine III
DARPA/NMRO
1400 Wilson Boulevard
Arlington, VA 22209-2308

Paul Johnson
ESS-4, Mail Stop J979
Los Alamos National Laboratory
Los Alamos, NM 87545

Mr. James C. Battis
GL/LWH
Hanscom AFB, MA 01731-5000

Janet Johnston
GL/LWH
Hanscom AFB, MA 01731-5000

Dr. Robert Blandford
DARPA/NMRO
1400 Wilson Boulevard
Arlington, VA 22209-2308

Dr. Katharine Kadinsky-Cade
GL/LWH
Hanscom AFB, MA 01731-5000

Eric Chael
Division 9241
Sandia Laboratory
Albuquerque, NM 87185

Ms. Ann Kerr
IGPP, A-025
Scripps Institute of Oceanography
University of California, San Diego
La Jolla, CA 92093

Dr. John J. Cipar
GL/LWH
Hanscom AFB, MA 01731-5000

Dr. Max Koontz
US Dept of Energy/DP 5
Forrestal Building
1000 Independence Avenue
Washington, DC 20585

Mr. Jeff Duncan
Office of Congressman Markey
2133 Rayburn House Bldg.
Washington, DC 20515

Dr. W.H.K. Lee
Office of Earthquakes, Volcanoes,
& Engineering
345 Middlefield Road
Menlo Park, CA 94025

Dr. Jack Evernden
USGS - Earthquake Studies
345 Middlefield Road
Menlo Park, CA 94025

Dr. William Leith
U.S. Geological Survey
Mail Stop 928
Reston, VA 22092

Art Frankel
USGS
922 National Center
Reston, VA 22092

Dr. Richard Lewis
Director, Earthquake Engineering & Geophysics
U.S. Army Corps of Engineers
Box 631
Vicksburg, MS 39180

Dr. T. Hanks
USGS
Nat'l Earthquake Research Center
345 Middlefield Road
Menlo Park, CA 94025

James F. Lewkowicz
GL/LWH
Hanscom AFB, MA 01731-5000

Dr. James Hannon
Lawrence Livermore Nat'l Laboratory
P.O. Box 808
Livermore, CA 94550

Mr. Alfred Lieberman
ACDA/VI-OA State Department Bldg
Room 5726
320 - 21st Street, NW
Washington, DC 20451

Stephen Mangino
GL/LWH
Hanscom AFB, MA 01731-5000

Dr. Frank F. Pilotte
HQ AFTAC/TT
Patrick AFB, FL 32925-6001

Dr. Robert Masse
Box 25046, Mail Stop 967
Denver Federal Center
Denver, CO 80225

Katie Poley
CIA-OSWR/NED
Washington, DC 20505

Art McGarr
U.S. Geological Survey, MS-977
345 Middlefield Road
Menlo Park, CA 94025

Mr. Jack Rachlin
U.S. Geological Survey
Geology, Rm 3 C136
Mail Stop 928 National Center
Reston, VA 22092

Richard Morrow
ACDA/VI, Room 5741
320 21st Street N.W
Washington, DC 20451

Dr. Robert Reinke
WL/NTESG
Kirtland AFB, NM 87117-6008

Dr. Keith K. Nakanishi
Lawrence Livermore National Laboratory
P.O. Box 808, L-205
Livermore, CA 94550

Dr. Byron Ristvet
HQ DNA, Nevada Operations Office
Attn: NVCG
P.O. Box 98539
Las Vegas, NV 89193

Dr. Carl Newton
Los Alamos National Laboratory
P.O. Box 1663
Mail Stop C335, Group ESS-3
Los Alamos, NM 87545

Dr. George Rothe
HQ AFTAC/TGR
Patrick AFB, FL 32925-6001

Dr. Kenneth H. Olsen
Los Alamos Scientific Laboratory
P.O. Box 1663
Mail Stop C335, Group ESS-3
Los Alamos, NM 87545

Dr. Alan S. Ryall, Jr.
DARPA/NMRO
1400 Wilson Boulevard
Arlington, VA 22209-2308

Howard J. Patton
Lawrence Livermore National Laboratory
P.O. Box 808, L-205
Livermore, CA 94550

Dr. Michael Shore
Defense Nuclear Agency/SPSS
6801 Telegraph Road
Alexandria, VA 22310

Mr. Chris Paine
Office of Senator Kennedy
SR 315
United States Senate
Washington, DC 20510

Dr. Albert Smith
Los Alamos National Laboratory
L-205
P. O. Box 808
Livermore, CA 94550

Colonel Jerry J. Perrizo
AFOSR/NP, Building 410
Bolling AFB
Washington, DC 20332-6448

Donald L. Springer
Lawrence Livermore National Laboratory
L-205
P. O. Box 808
Livermore, CA 94550

Mr. Charles L. Taylor
GL/LWG
Hanscom AFB, MA 01731-5000

DARPA/RMO/Security Office
1400 Wilson Boulevard
Arlington, VA 22209

Mr. Steven R. Taylor
Lawrence Livermore National Laboratory
L-205
P. O. Box 808
Livermore, CA 94550

Geophysics Laboratory
Attn: XO
Hanscom AFB, MA 01731-5000

Dr. Eileen Vergino
Lawrence Livermore National Laboratory
L-205
P. O. Box 808
Livermore, CA 94550

Geophysics Laboratory
Attn: LW
Hanscom AFB, MA 01731-5000

Dr. Thomas Weaver
Los Alamos National Laboratory
P.O. Box 1663, Mail Stop C335
Los Alamos, NM 87545

DARPA/PM
1400 Wilson Boulevard
Arlington, VA 22209

J.J. Zucca
Lawrence Livermore National Laboratory
P. O. Box 808
Livermore, CA 94550

Defense Technical Information Center
Cameron Station
Alexandria, VA 22314 (5 copies)

GL/SULL
Research Library
Hanscom AFB, MA 01731-5000 (2 copies)

Defense Intelligence Agency
Directorate for Scientific
& Technical Intelligence Attn: DT1B
Washington, DC 20340-6158

Secretary of the Air Force
(SAFRD)
Washington, DC 20330

AFTAC/CA
(STINFO)
Patrick AFB, FL 32925-6001

Office of the Secretary Defense
DDR & E
Washington, DC 20330

TACTEC
Battelle Memorial Institute
505 King Avenue
Columbus, OH 43201 (Final Report Only)

HQ DNA
Attn: Technical Library
Washington, DC 20305

DARPA/RMO/RETRIEVAL
1400 Wilson Boulevard
Arlington, VA 22209

CONTRACTORS (Foreign)

Dr. Ramon Cabre, S.J.
Observatorio San Calixto
Casilla 5939
La Paz, Bolivia

Prof. Hans-Peter Harjes
Institute for Geophysik
Ruhr University/Bochum
P.O. Box 102148
4630 Bochum 1, FRG

Prof. Eystein Husebye
NTNF/NORSAR
P.O. Box 51
N-2007 Kjeller, NORWAY

Prof. Brian L.N. Kennett
Research School of Earth Sciences
Institute of Advanced Studies
G.P.O. Box 4
Canberra 2601, AUSTRALIA

Dr. Bernard Massinon
Societe Radiomana
27 rue Claude Bernard
75005 Paris, FRANCE (2 Copies)

Dr. Pierre Mecheler
Societe Radiomana
27 rue Claude Bernard
75005 Paris, FRANCE

Dr. Svein Mykkeltveit
NTNF/NORSAR
P.O. Box 51
N-2007 Kjeller, NORWAY

FOREIGN (Others)

Dr. Peter Basham
Earth Physics Branch
Geological Survey of Canada
1 Observatory Crescent
Ottawa, Ontario, CANADA K1A 0Y3

Dr. Eduard Berg
Institute of Geophysics
University of Hawaii
Honolulu, HI 96822

Dr. Michel Bouchon
I.R.I.G.M.-B.P. 68
38402 St. Martin D'Herès
Cedex, FRANCE

Dr. Hilmar Bungum
NTNF/NORSAR
P.O. Box 51
N-2007 Kjeller, NORWAY

Dr. Michel Campillo
Observatoire de Grenoble
I.R.I.G.M.-B.P. 53
38041 Grenoble, FRANCE

Dr. Kin Yip Chun
Geophysics Division
Physics Department
University of Toronto
Ontario, CANADA M5S 1A7

Dr. Alan Douglas
Ministry of Defense
Blacknest, Brimpton
Reading RG7-4RS, UNITED KINGDOM

Dr. Roger Hansen
NTNF/NORSAR
P.O. Box 51
N-2007 Kjeller, NORWAY

Dr. Manfred Henger
Federal Institute for Geosciences & Nat'l Res.
Postfach 510153
D-3000 Hanover 51, FRG

Ms. Eva Johannisson
Senior Research Officer
National Defense Research Inst.
P.O. Box 27322
S-102 54 Stockholm, SWEDEN

Dr. Fekadu Kebede
Seismological Section
Box 12019
S-750 Uppsala, SWEDEN

Dr. Tormod Kvaerna
NTNF/NORSAR
P.O. Box 51
N-2007 Kjeller, NORWAY

Dr. Peter Marshal
Procurement Executive
Ministry of Defense
Blacknest, Brimpton
Reading FG7-4RS, UNITED KINGDOM

Prof. Ari Ben-Menahem
Department of Applied Mathematics
Weizman Institute of Science
Rehovot, ISRAEL 951729

Dr. Robert North
Geophysics Division
Geological Survey of Canada
1 Observatory Crescent
Ottawa, Ontario, CANADA K1A 0Y3

Dr. Frode Ringdal
NTNF/NORSAR
P.O. Box 51
N-2007 Kjeller, NORWAY

Dr. Jorg Schlittenhardt
Federal Institute for Geosciences & Nat'l Res.
Postfach 510153
D-3000 Hannover 51, FEDERAL REPUBLIC OF
GERMANY